Simulating Preferential Flow by A Multi-dimensional Process-based HYDRUS Model

Ying Zhao[1,2,*], Jun Yi[3], Rongjiang Yao[4], Fei Li[5], Robert Lee Hill[6]

[1]College of Resources and Environmental Engineering, Ludong University, Yantai 264025, China; [2]Global Institute for Water Security, University of Saskatchewan, Saskatoon, Saskatchewan, Canada; [3]Hubei Province Key Laboratory for Geographical Process Analysis and Simulation, Central China Normal University, Wuhan 430079, China; [4]State Key Laboratory of Soil and Sustainable Agriculture, Institute of Soil Science, Chinese Academy of Sciences, Nanjing 210008, China; [5]Grassland Research Institute, Chinese Academy of Agricultural Sciences, Huhhot 010010, China; [6]Department of Environmental Science and Technology, University of Maryland, College Park, MD 20742, USA.

[*]Corresponding author: yzhaosoils@gmail.com (Y. Zhao)

Abstract: Preferential flow processes are controlled by subsurface structures with the hierarchical organization across scales, but there is a lack of multiscale model validation using the field data. In this study, using a comprehensive dataset collected in the forested Shale Hills catchment, we tested and validated preferential flow occurrence by 2-dimension HYDRUS-2D at the hillslope scale, and in comparison, with 1-dimension HYDRUS-1D at the pedon scale and 3-dimension HYDRUS-3D at the catchment scale. There was good agreement between the 1D simulations and measurements of soil moisture in the soil profile, which was mainly affected by the vertical change in porosity/permeability with depth and precipitation characteristics; however, short-term fluctuations due to preferential flow were poorly captured. Notably, 2D and 3D simulations, accounting for preferential flow controlled by slope positions and shallow fractured bedrock, provided better results than the 1D simulations. Furthermore, a dual-porosity or anisotropic model provided more accurate predictions of soil moisture than a single-porosity or isotropic model due to a more realistic representation of local soil and fractured shale structure, which is also the premise of preferential flow (PF) occurrence. Consequently, our study reflected the central importance of multi-dimensional model approaches while highlighting the quantification of the soil structure and fractured nature of the bedrocks itself is essential to the simulation of preferential flow. The multi-dimensional modeling approaches can provide the mechanic presentation of PF pathways to the first-order stream and the necessity of the 3D simulation with detailed information to identify the dominant hydrological process.

Keywords: Hydrological processes; Preferential flow; Multi-dimensional Model; Fracture bedrock; HYDRUS

Soil is a three-dimensional structural unit affected by preferential flow processes under varying precipitation inputs, soil-terrain attributes, and moisture conditions. Preferential flow (PF), defined by Hendrickx and Flury (2001) as 'all phenomena where water and solutes move along certain pathways, while bypassing a fraction of the porous matrix', results in irregular wetting patterns in which water move faster in certain parts of the soil profile than in others (Freeze, 1972). Understanding the dynamics of PF is critical for explaining water flow through soils, the design of monitoring schemes, and for formulating models (Lin and Zhou, 2008; Clark et al., 2015). In the early periods, hydrology was considered one-dimensional and neglected the three-dimensional (3D; vertical + lateral) subsurface water flow (Fan et al., 2019). It is necessary to include PF phenomena such as fast transport through macropores, furrow flow due to the spatial variability of hydraulic properties, and fingering flow due to the instability of wetting fronts (Vogel and Roth, 2003; Vereecken et al., 2015; Gao et al., 2018).

Although PF is ubiquitous in hydrology, its proper identification and representation in hydrological models remain a challenge (Schulz et al., 2006; Beven and Germann, 2013; Clark et al., 2015; Gu et al., 2018). The PF and their subsequent processes are intimately related to the spatial structure of the subsurface heterogeneities caused by biologic or geological activities and geomorphological and soil-forming processes (Beven and Germann, 1982; Nimmo, 2012; Beven and Germann, 2013; Liu and Lin, 2015). This often presents over a hierarchy of scales and affect PF from the soil pedon up to the catchment scale (Blöschl and Grayson, 2001; McDonnell et al., 2007; Korres et al., 2015). In general, three distinctive scales are recognized. They are represented by three different conceptual and physical models for water flow in the vadose zone: pore scale, Darcian scale, and catchment scale (Hendrickx and Flury, 2001). A typical pore-scale PF is saturated, and unsaturated water flows through macropores and fractures. At the Darcian scale, unstable flow occurs in water repellent soils and layered soil profiles, and PF can also be induced by variability in soil hydraulic properties. At the areal scale, surface depressions and discontinuous layers with lower or higher permeabilities can cause PF. When multiple spatial scales are involved, the features at a smaller scale often form boundary conditions for the processes acting at a larger scale (Bittelli et al., 2010).

Up to now, the scales of spatial simulation models are usually too large to include the effects of lateral flow on soil water (Fan et al., 2019). Whatever the representative area of a model

domain is, the critical issue is whether the model code can define the complex but truly pedological and hydrological processes, assuming similar media scaling theory. Several studies have been conducted to compare various codes and approaches describing equilibrium water flow in the vadose zone (e.g., Scanlon et al., 2002), similar comparisons simulating preferential and nonequilibrium flow are lacking (Larsson and Jarvis, 1999). Especially, few models have developed to quantify those effects of heterogeneity and topography combined with scaling issues on hydrological fluxes (Ebel et al., 2007; Bittelli et al., 2010; Clark et al., 2015). Modelers generally rely on plot-scaled physical descriptions of water flow to describe the hillslope scale water balance (Tromp-van Meerveld and Weiler, 2008). Comparisons of 2D and 3D simulations of lateral convergence flow have shown that 3D simulation provides significantly better results (Loague et al., 2006; Mirus et al., 2007; Fan et al., 2019).

Another challenge of hydrological models is assessing various uncertainties, such as expressions of soil and bedrock features and boundary conditions (Loos et al., 2007). While previous research has mostly concentrated on uniform water flow with a single-porosity model, many experiments have demonstrated the presence of nonequilibrium flow with dual-porosity models (Beven and Germann, 1982; Durner, 1994; Šimůnek et al., 2006). For instance, laterally oriented macropore flow may dominate in areas where the macropores are created by plant roots (Newman et al., 1998; Gao et al., 2018). Especially in models of water movement in complex landscapes, lateral flow due to differences either in anisotropic hydraulic conductivity or topography should be taken into account (Buttle and McDonald, 2002; Maxwell and Kollet, 2008). Besides, lateral flow occurring at the interface between soil and bedrock and/or at the soil and hydrologically-impeding layers such as fragipans, has been recognized as an essential contributor to hillslope flow paths (e.g., Freer et al., 1997; Haga et al., 2005; Fan et al., 2019). However, only a few models have included a permeable soil-bedrock interface, and even fewer have tested this assumption with measurement data (Todd et al., 2000; Ebel et al., 2007; Camporese et al., 2019). Using some virtual experiments with a 3D physics-based model, Hopp and McDonnell (2009) systematically investigated the interactions between some of the dominant controls on subsurface stormflow generation. However, their model still lacked predictions of PF that could have been validated with actual measurements.

To clarify the extent and processes of PF, we investigated a forested Shale Hills watershed, characterized by the available high temporal and spatial resolution of soil moisture measurements. Previous studies at this critical zone observation site showed that the various landscape elements differ significantly in soil texture and structure with no systematic trend (Lin and Zhou, 2008; Guo et al., 2014), and PF was frequent (Zhao et al., 2012; Liu et al., 2015). We postulate that incorporating different soil types and their detailed spatial distributions into a physically-based model will enhance understanding of water flow mechanisms and predictability of PF. For this reason, we employed the Richards equation-based numerical model HYDRUS (Šimůnek et al., 2006), which includes a hierarchical system of various approaches simulating PF in the vadose zone. HYDRUS is well tested and widely used in diverse applications (Scanlon et al., 2002; Kohne et al., 2004; Saito et al., 2006; Twarakavi et al., 2008; Šimůnek et al., 2016). One of the remaining questions is whether this small-scale physics-based model, fed with accurate data, can adequately simulate the behavior of complex hydrological systems (e.g., PF) at a relatively large scale (Vereecken et al., 2015). In contrast, the previous larger-scale high-resolution models are still far from capturing the impacts of hillslope-scale structures on PF (Fan et al., 2019). Another similar question is how much complexity of dimension is needed in hydrological models, particularly in terms of conceptual clarity and computational efficiency (Tromp-van Meerveld and Weiler, 2008). Fan et al. (2019) considered that, in contrast to the 1-D, few-meters deep, and free-draining soil hydrology in most earth system models, 3-D, lateral ridge-to-alley flow through shallow and deep paths is the top globally quantifiable organizers of water and energy (and vegetation) within a model domain.

In this study, we focus our attention on examining the influence of spatial scale, soil porosity and anisotropy, and bedrock permeability on the development of PF. Our objectives are: (1) to assess the capabilities of multi-dimensional modeling in identifying the critical processes and parameters governing PF, (2) to evaluate the ability of the dual-porosity and anisotropic models to describe mechanisms of PF, and (3) to elucidate how soil-bedrock conditions affect PF occurrence from top-ridge to the first-order stream. The elements have been well tested individually but not previously applied in such an integrated manner for water resources or environmental modeling applications.

Materials and Methods

Experimental Site and Measurements

The model simulations presented here were based on field monitoring carried out at a 7.9-ha forested Shale Hills catchment, situated in central Pennsylvania, USA (Fig. 1), for four years from 2007 to 2010. Soil moisture monitoring indicated the existence of PF, which was influenced by soil properties such as soil type, soil depth, permeability, and soil location.

Experimental Site

The Shale Hills catchment has a typical humid continental climate, with a minimum mean monthly temperature of –3°C in January, a maximum mean monthly temperature of 22°C in July, and annual precipitation of about 980 mm (National Weather Service, State College, PA). The V-shaped catchment is drained by a first-order stream in the valley and has moderately steep slopes of up to 25–48% on both sides of the stream. Elevation ranges from 256 m at the outlet of the catchment to 310 m at the highest ridge. The catchment is underlain by about 300-m thick, steeply bedded, highly fractured Rose Hill Shale, and covered by maple-oak-hickory forest. The soils have a silt loam and silty clay loam texture, which were formed from shale colluvium or residuum, with many channel shale fragments throughout most of the soil profiles (Table 1).

Field monitoring

For the in-situ monitoring, sensors were installed at four sites (Figure 1, Table 1), which characterized by the four soil series: Weikert series on a hilltop (Site 74), Berks series at a mid-slope (Site 53), Rushtown series at the downslope of a swale (Site 51), and Blairton series close to the first-order stream that is at the outlet of a swale (Site 15). An array of sensors was installed at each site to measure soil water content, soil matrix potential, and soil temperature by soil horizons. For the PF analysis, this paper mainly focused on the soil moisture data obtained at 10-minute intervals using the ECH_2O probes (Decagon Devices, Inc., Pullman, WA) with an accuracy of ±3% and a measurement resolution of 0.1%. Our previous reports had identified a PF to occur when a subsurface soil horizon responded to a rainfall input earlier than a soil horizon above it (Lin and Zhou, 2008). Here we take the monitoring data we also used for the model test as an example. Figure 2 shows that the underlying R horizon responses to the storm events while overlying soil horizons did not respond at site 74 near the hilltop. At site 51 in the middle of a swale, a rapid 2.0% increase in soil moisture was apparent at 0.18- and 0.25-m depths in the B horizon, while soil moisture in the horizons above and below the B horizon did not change similarly. Intuitively, when a

soil moisture sensor buried in a subsoil responded to a storm event earlier than other sensors above it, the water likely bypassed the overlying horizon(s) (i.e., vertical PF) or had infiltrated into the deeper subsoil from the upslope or side-slope areas (i.e., lateral PF). We wish to make it quite clear that using the wording "preferential flow (PF)" implies structures that permit all types of macropore flow, unstable flow, funnel flow, etc. We recognized that there is no formulation of criteria for determining PF occurrence (Hendrickx and Flury, 2001; Nimmo, 2012). Our method might underestimate the occurrence of PF since it does not necessarily require all the phenomena accounted for by our analysis.

Measurements

To determine soil hydraulic properties (Table 2), representative soil horizons were sampled from each soil pit. Saturated hydraulic conductivities (K_s) were determined with the falling head method using large, 30-cm diameter, undisturbed cores taken near the study hillslope (Lin et al., 2006). Besides, the anisotropic K_s is also accounted for, in which large differences in the lateral and vertical K_s have been found, e.g., the horizontal K_s 10 times higher than the vertical one in the B layer and the vicinity of the bedrock fractures (Table 2). This difference is ascribed to a platy structure due to the geological formation of a long horizontal axis leading to a higher continuity in the horizontal direction along the aggregates/fractures. The water retention characteristics were determined by the pressure plate method, and parameters were fitted using RETC (van Genuchten et al., 1991). The soil texture, bulk density, and total C-content were determined using disturbed soils (Zhao et al., 2010). The precipitation and weather variables required to estimate potential evapotranspiration were recorded by an *in-situ* automatic micrometeorological station. Root density, LAI, and coverage of trees were also recorded monthly in this catchment. The groundwater sensor is installed at site 15, and discharge is measured at the lower outlet stream gauge of the catchment (Fig. 1a).

Model Evaluation in Simulation of Preferential Flow

In this study, we used the HYDRUS codes (1D, 2D, and 3D) for the water movement simulations (Šimůnek et al., 2006). Practically, we used the HYDRUS-2D as a baseline of the model (i.e., the common model approach) and compared it with the HYDRUS-1D (standard vertical fluxes) and HYDRUS-3D (most complex flux) when the model scale issues were involved (Table 3). Furthermore, based on the calibrated HYDRUS-2D, we assessed the model uncertainties such as expressions of soil and bedrock features and boundary conditions, in predicting the PF.

Governing Flow Equation

The HYDRUS-2/3D solves the Richards' equation for uniform water flow in saturated/unsaturated domains. The governing flow equation is a modified form of Richard's equation given as:

$$\frac{\partial \theta}{\partial t} = \frac{\partial}{\partial x_i}\left(K(K_{ij}^A \frac{\partial h}{\partial x_j} + K_{iz}^A)\right) - S \qquad [1]$$

where θ is the volumetric water content ($L^3 L^{-3}$), h is the pressure head (L), S is a sink term (T^{-1}), x_i (i = 1, 2, 3) are the spatial coordinates (L), t is time (T), and K_{ij}^A and K_{iz}^A are components of a dimensionless anisotropy tensor K^A, and K is the unsaturated hydraulic conductivity ($L\ T^{-1}$), respectively. We used the conventional van Genuchten-Mualem model (van Genuchten, 1980) for the hydraulic functions as follows:

$$S_e = \frac{\theta - \theta_r}{\theta_s - \theta_r} = \frac{1}{(1+|\alpha h|^n)^m} \qquad [2a]$$

$$K = K_s S_e^l [1-(1-S_e^{1/m})^m]^2 \qquad [2b]$$

where S_e is the effective saturation, θ_s and θ_r are the saturated and residual water contents (L^3 L^{-3}), respectively; the symbols α (L^{-1}), n, and m = 1-1/n are empirical shape parameters; K_s is the saturated hydraulic conductivity ($L\ T^{-1}$), and l is a pore connectivity parameter which usually is set to 0.5.

In comparison with the uniform single-porosity model (Eq. 1), a nonequilibrium dual-porosity model is also used, which assume that water flow is partitioned into a macropore or fracture domain (the inter-aggregate pore domain) and a matrix domain (the intra-aggregate pore domain) where the water does not move at all (Šimůnek et al., 2003). This conceptualization leads to a two-region type flow models that partition the liquid phase into mobile (flowing, inter-aggregate), θ_{mo}, and immobile (stagnant, intra-aggregate), θ_{im}, regions [L^3 L^{-3}]: $\theta=\theta_{mo}+\theta_{im}$. The dual-porosity formulation for water flow can be represented as (Gardenas et al., 2006):

$$\frac{\partial \theta_{mo}}{\partial t} = \frac{\partial}{\partial x_i}\left(K_{ij} \frac{\partial h}{\partial x_j} + K_{iz}\right) - S_{mo} - \Gamma_w \qquad [3a]$$

$$\frac{\partial \theta_{im}}{\partial t} = -S_{im} + \Gamma_w \qquad [3b]$$

where S_{mo} and S_{im} are sink terms for the mobile and immobile regions, respectively [T^{-1}], and Γ_w is the water transfer rate between the inter- and intra-aggregate pore domains [T^{-1}]. The water mass transfer rate in [3b] is assumed to be proportional to the difference of the pressure head between the macropore and matrix regions (Gerke and van Genuchten, 1993b):

$$\Gamma_w = \alpha_w (h_f - h_m) \quad [3c]$$

where a_w is a first-order mass transfer coefficient ($L^{-1}T^{-1}$):

$$\alpha_w = \frac{\beta}{d^2} K_a(h) \gamma_w \quad [3d]$$

where d is an effective diffusion path-length (i.e., half the aggregate width) (L), β is a shape factor that depends on the geometry of the soil aggregates (-), γ_w is a scaling factor (-), and K_a is the effective hydraulic conductivity of the fracture–matrix interface ($L\ T^{-1}$) determined as a simple arithmetic average involving both h_f and h_m as:

$$K_a(h) = 0.5[K_a(h_f) - K_a(h_m)] \quad [3e]$$

Model Domain, Initial, and Boundary Conditions

We designed the 3D simulated domain of 85 m length, 3 to 8 m width, and 1 to 4 m depth with a slope from 7% to 38% (Fig. 1 and Table 1). Based on soil horizon, the soil profiles were divided into 18 materials characterized by depth-related soil hydraulic parameters, with four layers for the hilltop and four layers mid-slope, five layers down-slope (swale) and five layers outlet parts, respectively. Based on this, the 2D simulation domain was considered as transect without width, and 1D simulation was the vertical soil profile with the heterogeneous soil layers at each of the four locations. The 3D model domain was implemented by importing the Shale Hills hillslope DEM (digital elevation model; x-, y-, z-coordinates of the surface and bedrock topography). The DEM of the catchment was interpolated from light detecting and ranging (LiDAR) elevation point clouds collected by an airplane flown over the catchment in 2006 (PAMAP, PA Department of Conservation and Natural Resources). Approximately 40,000 LiDAR elevation points were interpolated into a 1 m x1 m DEM using ArcGIS 9.2 (ESRI Inc., Redland, CA, USA). Based on this geometric information, we generated a finite element mesh containing 46,200 nodes and resulted in 80,959 3D elements (grid cells) in the form of triangular prisms. The transition into the deeper bedrock was represented by an inclined planar base surface (Fig. 1b). A triangular grid did the discretization of the model area with the intersections of the adjoined triangles referred to as nodes. The grid was spaced <1 cm in the soil domain to ensure numerical stability, with the grid being denser in the topsoil and at the boundaries between layers.

Model initial conditions were set by linear interpolation of soil moisture at different depths measured at the beginning of the simulation date. The measured daily rainfall and calculated potential evapotranspiration (PET) via the Hargreaves equation were used as a time-variable

atmospheric upper boundary condition (BC) of the model domain. Precipitation and PET were additionally corrected for the interception (Šimůnek et al., 2006). The upslope boundary and the two-edges of the domain along the slope were treated as no flux boundaries. A seepage face BC was assigned to the entire width of the lower part of the domain, allowing water to leave the domain under zero potential. A free drainage lower BC was specified for the bottom of the model domain, assuming a unit total vertical hydraulic gradient. The minimum allowed pressure head was considered as 1500 kPa at the upper BC. Root water uptake was based on the model of Feddes et al. (1978). In general, the maximum rooting depth was designed to be 100 cm, with the greatest root density in the upper 50-cm soil depth.

Model Calibration and Implementation

Our multi-dimensional modeling approach essentially corresponds to the three types of PF that occurred in three scales. In the 1D simulation at the pedon scale, depth-related hydraulic parameters represent unstable water flow due to the heterogeneous soil layers (e.g., macropore flow). In the 2D simulation at the hillslope scale, we further considered the subsurface lateral flow from different sloped positions (e.g., funnel flow due to impeding layer). The 3D simulation at the catchment scale allowed us to consider lateral convergence flow from the surrounding units. To compare different model approaches, the hydraulic properties and boundary conditions for each simulation were parameterized as consistently as possible with independent measurements (Table 3). We first calibrated the HYDRUS-2D model using the two-month data from July and August in 2007 (Fig. 3). For that calibration step, the measured soil hydraulic parameters (i.e., uncalibrated parameters) were used as initial values for the simulations. Table 1 showed that soil horizons varied from loamy sand to sandy loam. The changes in the soil texture also reflect changes in the total porosity and the pore size distribution, as indicated by the depth-related hydraulic parameters (Table 2). For instance, the Weikert soil had a lower saturated water content (θ_s) and a shallow R horizon while Rushtown had a large θ_s and a deep soil depth. We then did the inverse model to optimize the hydraulic parameters. The van Genuchten-Mualem parameters α, n, and K_s were adjusted during the calibration process based on our soil profile moisture measurements at the monitoring sites (Table 2). The calibrated parameters showed much better simulations than the measured one; that is, the peak and range of measured soil water were simulated reasonably (Fig. 3). Therefore, we used the calibrated parameters for all subsequent HYDRUS simulations.

Temporal simulation setting

Although model calibration represented one level of testing to reproduce field data, the model may not be applied to field conditions that are significantly different than the conditions under which calibration was conducted. As also indicated by Melsen et al. (2016), the model calibration and validation time interval should keep pace with the increase in spatial resolution to resolve the processes that are relevant at the applied spatial resolution. For these reasons, it is important to test the predictive capabilities beyond the calibration period. Based on data availability, we designed the simulation time for three temporal scales to cross-examine modeling for various scenarios. The first time scale was minute-based representing the rapid response of water redistribution after rainfall, used to evaluate the occurrence of PF. The second time scale was daily-based, representing the water dynamics associated with cycles of wetting and drying within a hydrological year and was used basically to calibrate and validate the modeling. The third time scale was yearly-based representing the water cycles over multiple years, used to check the power of model predictions for long-term periods.

Model Uncertainties

The simulations of hydrological fluxes are affected by various uncertainties resulting from the soil hydraulic parameterization and boundary conditions (Loos et al., 2007). Firstly, the above-calibrated parameters α, n, and K_s in the single-porosity model were then used as default values for calibration of the dual-porosity model, where only a_w was fitted while others (i.e., θ_s and θ_r) were modified corresponding with the single-porosity model (Table 2). The residual water content is equal to zero for the mobile region (i.e., residual water only present in the immobile region; Clothier et al., 1995). Secondly, to illustrate the consequences of anisotropic hydraulic properties on PF, the model results using anisotropic K_s are compared with the model output from isotropic K_s. For some unmeasured horizontal K_s that are attributed to the fractured bedrock, we used a value that is 10 times the vertical K_s. Thirdly, to examine the effect of fractured shale bedrock, the lower BC was set as either a highly-weathered permeable bedrock (i.e., free drainage) or less-weathered, impermeable part (i.e., no flux) (Tromp-van Meerveld et al., 2007).

Performance Assessment

In addition to graphical displays of simulated and measured results, statistical measures (root mean square error, *RMSE*, and the Nash–Sutcliffe efficiency, *NSE*) were used to evaluate the model performance (e.g., Ebel et al., 2007; Bittelli et al., 2010), as follows:

$$RMSE = \sqrt{\frac{1}{N}\sum_{i=1}^{N}(P_i - O_i)^2} \quad [4a]$$

$$NSE = 1 - \frac{\sum_{i=1}^{N}(P_i - O_i)^2}{\sum_{i=1}^{N}(O_i - \bar{O})^2} \quad [4b]$$

where N is the number of observations, P_i and O_i are the simulated and measured values, respectively, and $\bar{O}$ is the mean of the observed values, respectively. The *RMSE* is inversely proportional to model efficiency with smaller *RMSE* values indicating higher model efficiency. The *NSE* efficiency statistic ranges between -∞ and 1, with 1 indicating a perfect match between observed and modeled values and less than zero indicating that the predicated value results in more error than using the average value of the observations.

Results

Performance of Multi-dimensional Modeling Approach

Soil moisture was simulated using a multi-dimensional modeling approach for three temporal scales (Figs. 4-6). Regardless of the model approaches, the model performed well in simulating soil moisture trends. We found that the most complex model provided the best predictions of the measured dynamics at each monitoring site. The PF was successfully described by 2D or 3D modeling approaches, but not by 1D simulation (Fig. 4). Notably, 3D modeling simulated the timing of the PF occurrences accurately. While the 3D Richards equation-based numerical model simulated water increases at the R horizon earlier than the above soil layer, the 1D simulation showed the frequent increase from top to down soil at site 74. Similarly, at site 51, the 3D simulation showed very well matched to the measured soil moisture at the 40-cm soil depth, which is much earlier and large increases than the above 18-cm soil depth; however, the 1D simulation did not reflect the occurrence of PF. However, even that 3D simulations at site 74 lagged about 6 h behind the measured data at the R horizon, in which water bypassed the upper horizons and reached the subsoil probably related to the water repellency of the organic litter or water recharges originated in the side slope (Lin et al., 2006). Our current model still did not take account of those processes well. The *RMSE* values are all smaller than 0.1, with the 3D simulations having the lowest bias and the 1D simulations having the highest bias (Table 4). Similarly, the *NSE* values range from -3.8 to 0.74, with the 3D simulation having the most favorable expectations. The results in the

right part of Table 4 seem to agree with the trends previously observed in the figure. We noticed that some *NSE* values are below zero that may illustrate the effect of a few very poorly simulated values in biasing the *NSE*.

For 1-yr hydrological simulations (Fig. 5), the 1D model underestimated the soil moisture because it did not consider the lateral flow contributions. In contrast, the 2D simulation, which considered the sloped-topographic effects, has reflected the occurrence of PF. The 2D simulations did not perform as well as the 3D simulations when comparing daily soil moisture observations and simulations. The 3D simulations provided the best predictions of the measured values, although there are still some differences that are primarily attributed to the spatial variability inherent in hydrological processes (Fig. 5). Figure 6 showed the 2D simulation for the 4-yr period, which showed a very similar predictive power with the 1-yr simulation, indicating the current model can simulate the hydrological processes for the long-term period. Figure 7 shows the simulated water balance in 2007, indicated that 38% of the precipitation was drained (of which 6% was seepage flux and 32% was streamflow), 35% was evaporated, 19% was transpired, and 8% was stored in the soil. The overland flow was a small portion and only occurred after higher rainfall intensity events. Actual evapotranspiration was relatively large for the maple-oak-hickory vegetation compared to the amount of subsurface drainage.

The 3D model enabled predictions to be obtained for soil water content distributions at each location and time, considering convergent lateral inflows. An example of a 3D representation of pressure head on August 21, 2007 (Fig. 8), indicating a higher water potential in the downslope positions or the topsoil depths. Furthermore, we selected a transect of simulation on the same date to show representative subsurface lateral flow after rainfall events (Fig. 9). In this example, PF in the shallow Weikert soil occurred in the R horizon while in the deep soil such as the Rushtown, it happened in the Bw and C horizons. The increases in soil moisture indicate that the water infiltrated into the bedrock fractures below the shallow Weikert soil and moved laterally to the deep horizons of the downslope Rushtown soil. To our best knowledge, this is one of few attempts to capture the PF pathways by using the physically-based model successfully.

Effects of Soil Parameters and Boundary Condition

We firstly examined the significance of the nonequilibrium flow in a dual-porosity system. The single-porosity and dual-porosity approaches reflected the soil moisture dynamics throughout a hydrological year (Fig. 10). However, the dual-porosity model provided improved simulations, implying that the model in considering the fracture-matrix structure may have indicated that the area is characterized by a fractured structure, which is the premise of the PF. Besides, the prominence of PF may also be supported by the anisotropic K_s. Expectedly, Figure 11 shows that the simulations improved once the anisotropic K_s was considered, indicating that anisotropy significantly contributed to the rapid subsurface flow. Examination of Table 4 also confirms that the single-porosity model does not perform as well as the dual-porosity model, and considering anisotropic K_s improves the simulations.

Our results illustrated that the boundary condition is essential for PF simulation. At site 74, a no flux BC provided better predictions than when a permeable BC was assumed (Fig. 12a). However, at site 51, a free drainage BC provides better predictions than when an impermeable BC is taken into account (Fig. 12b). This implied that site 74 was characterized by an impermeable soil-bedrock interface (Table 4), whereas site 51 should be described by permeable shale geology. Furthermore, Figure 14a showed that the model performed well in simulating the water table dynamics at site 15, considering that perched water table and groundwater recharge into the soil may not be fully considered in our model. Furthermore, Figure 14b shows the measured discharge for the whole catchment and simulated discharge in the sub-catchment accounted for (i.e., our 3D domain). Although the values can not be directly compared, the similar trends and dynamics between them should have indicated that our model was sensitive in simulating lateral subsurface drainage from hills to valleys.

Discussion

Identification of Preferential Flow using a modeling approach

In our study, direct evidence of PF was obtained by comparing the dynamics in the measured soil moisture contents and further validated by the numerical simulations. The occurrence of PF is illustrated to be governed by internal properties and external influences. Expectedly, one-dimensional hydrological modeling has one general disadvantage in that lateral water fluxes may not be taken into account, in which the external influences are generally identified as input and output fluxes in the vertical dimension. Even the dual-porosity model in 1D

simulation, it still failed to capture the macroflow due to it exhibited the sequential flow in the soil profile (Larsson and Jarvis, 1999). During 2D simulation, lateral flow from ridges to valleys was correctly simulated, in which output fluxes from adjacent spatial units are commonly input fluxes to the neighboring spatial units and have been referred to as a catenary linkage along the slopes (Zepp et al., 2005). Our results recognized that the 2D simulations did not perform well as the 3D simulations predicted the PF. During the 3D simulations, the lateral convergence flow from the surrounding units strongly contributed to the PF dynamics, especially in the concave hillslope position (e.g., site 51). Those model findings are consistent with the previously observed analysis that lateral/inter-connected flow frequently occurred in this sloped forest (Grahamm and Lin, 2011). While the 3D physics-based modeling has previously been restricted in a complex landscape (Loague et al., 2006; Mirus et al., 2007), our study addressed the necessity to perform 3D simulations with the reasonable parametrization to describe the PF components and pathways adequately. Tromp-van Meerveld and Weiler (2008) indicated that the inclusion of PF in the model influenced the distribution of the maximum saturation depths at the soil-bedrock interface and increased peak flows and recessions. At their studied Panola hillslope, several process-based modeling studies have taken into account the detailed representation of hydrologic and hydrostratigraphic variables (Hopp and McDonnell, 2009; James et al., 2010; Camporese et al., 2019). However, their model did not strictly capture the PF dynamics, particularly in terms of validating with the field observations.

Effects of Soil Parameters in Simulating Preferential Flow

Numerous studies have shown that flow processes in soils can be better described using nonequilibrium two-domain models rather than classical single-domain models (e.g., Šimůnek et al., 2003; Kohne et al., 2004). Our results confirm that, in comparison with a single-domain model, dual-porosity models do perform well in describing the processes within the local soil subsurface macropore network and better represent the dynamics of soil moisture (McDonnell et al., 2007). Studies have also mentioned that soils consisting of fine layers parallel to the surface, like stratified soils, have a horizontal K_s that is greater than the vertical K_s (e.g., Newman et al., 1998; Beckwith et al., 2003). In the same studied area, Guo et al. (2019) showed that water movement is almost parallel to the lateral slope. This observation might explain why the simulations that consider the anisotropy of K_s produce better prediction results than that considered isotropic K_s. In our simulation, the contrast of

anisotropy is somewhat like the ratio of soil to bedrock in the fractured zone. It is expected that omitting the anisotropy in hydraulic parameters will negatively affect simulation results (Ebel et al., 2007; James et al., 2010). The inference is that the anisotropic K_s is more realistic in representing the macroporosity found in the structured soil and that the studied watershed was characterized by weathered and un-weathered bedrocks that contribute a lateral flow pathway.

Effects of Boundary Conditions in Simulating Preferential Flow

We demonstrated that the representation of fractured shale geology is essential to simulate the occurrence of PF accurately. Although the bedrock is typically assumed as an impermeable layer in numerical models, there is evidence indicating that bedrock sometimes is permeable (e.g., Comporese et al., 2019). Our results show that actual field conditions may be more accurately characterized by considering both a permeable fracture-structured shale bedrock (e.g., site 51) and an impermeable bedrock (e.g., site 74). This finding was corroborated by Ebel et al. (2007), who indicated that representing layered geologic interfaces by an impermeable boundary condition leads to significant prediction errors. Several other researchers have also documented the role of soil-bedrock interfaces as important hillslope flow paths (e.g., Freer et al., 1997; Onda et al., 2001). Lin et al. (2006) described a discontinuity in the fragipan and noted that a significant error in perched water depths could be caused by a minimal mistake in simulated soil water contents, and vice versa. In this regard, our inability to continuously parameterize the structure and geometry of sub-catchment may have prevented detailed assessments of the weathered bedrock water table response and discharge (Fig. 13), as well as the soil moisture dynamics. The more sophisticated geological characterization will be needed to improve model predictions (Rakovec et al., 2016).

Pathway and Connectivity along the Hillslope

It was determined that hyper-resolution monitoring data of soil moisture might be used to address the occurrence of PF at the point scale. Combined with a model survey, potential spatial flow patterns may be identified, flow mechanisms may be confirmed, and flow pathways may be documented at the hillslope scale (Sidle et al., 2001; Salve et al., 2012; Fan et al., 2019). The connectivity of flow paths is highly related not only to the soil-bedrock properties but also to the initial moisture content (Salve et al., 2012). Although PF occurred at

each site, only a few rainfall events led to connectivity from the hilltop to the valley floor (data in the supplement file; Lin and Zhou, 2008). Especially during the initial soil dry condition and/or combined the short-lasting and intense rainfall event, while lateral macropore flow was dominant in the planar uphill position, a combination of vertical macropore flow and lateral matrix flow was dominant in the concave midslope position. This suggested that during dry conditions, the flow paths for the occurrence of PF are only 'locally' connected and can be activated to deliver water through long distances to the valley floor (Guo et al., 2014), as illustrated by the simulation in Figure 8. It is also likely that a perched water table developed in the shallow subsurface and resulted in the water flow towards the downslope position, as was indicated by a rapid rise of topsoil water after large precipitation events at site 15 (Fig. 13a). The presence of a perched water table indicated that the vertical percolation locally exceeded the K_s at the perching layers and suggested that flow paths may not be vertical through the entire thickness of the unsaturated zone. Instead, water has diverted laterally to a fault zone or another high-permeability channel that channeled downward to the water table.

For a conceptual understanding of modeling findings, we present a flow diagram (Fig. 14) by summing up two types of subsurface lateral flow as dominating hydrological features, which were highly controlled by multiscale behavior of the intrinsic soil and fracture system. The first pathway that PF was initiated when the rainfall infiltrated the shallow impermeable bedrock at the upslope, where water moves laterally, recharged the Bw and C horizons of the mid-slope and downslope, and finally recharged the Bt horizon and the C horizon of the valley floor. A second pathway had water moving through the fracture and directly recharged the deep C horizon at the downslope and valley floor sites. This constituted a hydrological pathway for rapid lateral flow above the groundwater zone, especially during the initial soil wet condition, and/or associated with the long-lasting and intermittent rainfall.

Implications and Beyond of model simulation

In this study, we compared different conceptual approaches to simulate the PF paths in soils. Based on the monitoring evidence of PF and identification of geomorphological conditions, we explored an efficient model approach to confirm our former assumption that subsurface lateral flow is the primary flow mechanism in this catchment (Lin et al., 2006). The HYDRUS model results provide an excellent approximation that describes potential

hydrologic flow paths for a complex hillslope structure underlain by fractured bedrocks. The simulations reported herein demonstrate that Richards equation-based numerical models, like HYDRUS, can characterize detailed spatio-temporal hydrologic responses, developing the concepts of the process-based multiscale model, and representing PF paths. The field-based observations and hydrologic-response simulations from the Shale Hills catchment highlight the evidence in simulating fractured bedrock water flow within a complex small catchment and have important implications for understanding hydrologic response in these types of catchment basins.

In comparison with the previous researches, our modeling application led to several improvements: 1) the full 3D simulation parameterized by the detailed field observations, followed by validation via the experimental data, which provides greater feedback for the understanding of process-based concepts (Fan et al., 2019). In the past, it lacks in the evaluation of scales since we do not adequately perform on small-scale processes integrating up to larger scales (Beven et al., 2020), and thus a Richards equation-based model like HYDRUS may only be applied in the small scale or the relatively simple geomorphological conditions; 2) the characterization of soil hydraulic properties that includes PF via macropores and fractures, and a more accurate description of the subsurface as a multi-layer soil profile above the bedrock (Rakovec et al., 2016). Comparison of hydrologic-response simulations using lab measured soil-water retention curves versus inversely estimated parameters combined with the field moisture measurement showed that integrating soil data with detailed hydrological information (e.g., interflow) can dramatically improve the simulation; 3) the explicit consideration of the anisotropic hydraulic parameters that is virtually ignored in the hydrological calculations (McDonnell et al., 2007). This is a challengeable area given the near impossibility of making the field measurements to assess how soil anisotropy and bedrock permeability influence PF (James et al., 2010; Camporese et al., 2019); and 4) the variable representation of boundary conditions considering that our area, as well as many forest hillslopes composed of relatively thin, permeable soil mantles overlaying less-permeable bedrock (Camporese et al., 2019). In the previous study, lacking presentation of layered geologic interfaces with an assumption of impermeable BC leads to substantial inaccuracies.

Earth System Models are essential tools for understanding the dominant hydrological processes. Still, they cannot explicitly resolve the first-order structures and functions that

fundamentally organize water and energy across the landscapes (Fan et al., 2019). Recently, Camporese et al. (2019) confirmed that Richards equation-based numerical model (CATHY) could generate threshold-driven hillslope responses, e.g., fill and spill mechanism at Panola Mountain Research Watershed. It is promising to further investigate either whether the HYDRUS can reproduce threshold mechanisms or to what extent the fill and spill process exists in a well-gauged Shale Hills catchment. At the same catchment, based on the ground-penetrating radar survey, Guo et al. (2014) found that soil moisture at specific hillslope locations may work as necessary "nodes" and the soil horizon may function as a "path" in the subsurface flow network. They established a conceptual fill-and-spill model of subsurface runoff generation to describe the roles of PF in subsurface hydrology (Guo et al., 2019). Process understanding, data collection, and model development should be linked so that a complete representation can be obtained with each iteration (Grayson and Blöschl, 2000). Still, it is challenging to describe the finer-scaled (meters) principle hillslope structure representing by a physically-based model into the larger-scaled (kilometers) earth system model, which again recalled the scaling issue (Clark et al., 2017). Currently, the limited availability of the less-than-perfect observed data sets had restricted the field validation of PF models. Without detailed field measurements, it is unlikely that our modeling approach would have identified fractured bedrock flow as an essential process (Beven et al., 2020). Provided such data are available, our results indicate that physically-based models, like HYDRUS, when accurately parameterized, can simulate catchment-scale water flow (Fan et al., 2019).

Conclusions

In this showcase application, we compared increasingly complex models with a consistent dataset. We concluded that a multi-dimensional modeling approach helped to elucidate how PF processes are affected by soil-landscape features in a small catchment. The model results verified that detailed characterization of soil and bedrock thickness is critical for simulating pore-water pressure generation at sites like Shale Hills, where the convergent subsurface flow is essential. We found that: 1) when the PF was considered in 2D and 3D simulations, it improved the model predictions; 2) the dual-porosity model outperformed the single-porosity model since it can well delineate macropores in the soil, with consideration of anisotropic K_s further improving the model accuracy; and 3) models considering the presence of fractured bedrock performed better than when this was not considered and demonstrated that the actual

field conditions were characterized by fractured bedrock. Further study is expected to examine the robustness of the multi-dimensional process-based hydrological modeling under varying conditions.

Acknowledgments

This research was supported in part by the U.S. National Science Foundation through the Shale Hills Critical Zone Observatory grant (PI: Henry Lin; EAR-0725019), Taishan Scholars Program (201812096), and the National Natural Science Foundation of China (41977009). Fei Li was supported by the Agricultural Science and Technology Innovation Program of CAAS (CAAS-ASTIP-2020-IGR-04). Data were provided by the NSF-supported Southern Sierra Critical Zone Observatory. The data set is available at http://criticalzone.org/shale-hills/data/datasets/. Assistance in field data collections from the Penn State Hydropedology Group and suggestions of Markus Flury from Washington State University and Jeffrey J. McDonnell from the University of Saskatchewan are gratefully acknowledged.

References

Beckwith, C.W., A.J. Baird, and A.L. Heathwaite. 2003. Anisotropy and depth-related heterogeneity of hydraulic conductivity in a bog peat. II: Modelling the effects on groundwater flow. *Hydrological Processes*, 17, 103–113.

Beven, K., 2001. On explanatory depth and predictive power. *Hydrological Processes*, 15, 3069–3072.

Beven K., and P. Germann. 2013. Macropores and water flow in soils revisited. *Water Resources Research*, 49, doi:10.1002/wrcr.20156.

Beven K., and P. Germann. 1982. Macropores and water flow in soils. *Water Resources Research*, 18, 1311-1325.

Beven, K., Asadullah, A., Bates, P., Blyth, E., Chappell, N., Child, S., …and T., Wagener. 2020. Developing observational methods to drive future hydrological science: Can we make a start as a community? *Hydrological Processes*, 34, 868–873, https://doi.org/10.1002/hyp.13622.

Blöschl, G., and R.B. Grayson. 2001. Spatial Patterns in Catchment Hydrology: Observations and Modelling, 416 pp., Cambridge Univ. Press, New York.

622 Binley, A., Hubbard, S.S., Huisman, J.A., Revil, A., Robinson, D.A., Singha, K., and Slater,
623 L.D. 2015. The emergence of hydrogeophysics for improved understanding of
624 subsurface processes over multiple scales. *Water Resources Research*, 51, 3837–3866.
625 https//doi.org/10.1002/2015WR017016.
626 Bittelli, M., F. Tomei, A. Pistorcchi, M. Flury, J. Boll, E.S. Brooks, and G. Antolini. 2010.
627 Development and testing of a physically based, three-dimensional model of surface and
628 subsurface hydrology. *Advance in Water Resources*, 33, 106–122.
629 Buttle, J.M., and D.J. McDonald. 2002. Coupled vertical and lateral preferential flow on a
630 forested slope. *Water Resources Research*, 38:1060, doi:10.1029/2001WR000773.
631 Camporese, M., Paniconi, C., Putti, M., and McDonnell, J.J. 2019. Fill and spill hillslope
632 runoff representation with a Richards equation-based model. *Water Resources Research*,
633 55. https://doi.org/10.1029/2019WR025726.
634 Clark, M.P., Fan, Y., Lawrence, D.M., Adam, J.C., Bolster, D., Gochis, D.J., et al. 2015.
635 Improving the representation of hydrologic processes in Earth System Models. *Water*
636 *Resources Research*, 51, 5929–5956. https://doi.org/10.1002/2015WR017096.
637 Clark, M.P., Bierkens, M.F.P., Samaniego, L., Woods, R.A., Uijlenhoet, R., Bennett, K.E.,
638 Pauwels, V.R.N., Cai, X., Wood, A.W., and C.D. Peters-Lidard. 2017. The evolution of
639 process-based hydrologic models: historical challenges and the collective quest for
640 physical realism. *Hydrology and Earth System Sciences*, 21, 3427–3440.
641 Durner, W. 1994. Hydraulic conductivity estimation for soils with heterogeneous pore
642 structure. *Water Resources Research*, 30, 211–233.
643 Ebel, B.A., K. Loague, J.E. Vanderkwaak, W.E. Dietrich, D.R. Montgomery, R. Torres, and
644 S.P. Anderson. 2007. Near-surface hydrologic response for a steep, unchanneled
645 catchment near Coos Bay, Oregon: 2. Physics-based simulations. *America Journal of*
646 *Science*, 307, 709–748.
647 Fan, Y., Clark, M., Lawrence, D.M., Swenson, S., Band, L.E., Brantley, S. L., et al. 2019.
648 Hillslope hydrology in global change research and Earth System Modeling. *Water*
649 *Resources Research*, 55, 1737–1772. https//doi.org/10.1029/2018WR023903.
650 Feddes, R.A., P. Kabat, P.J.T. van Bakel, J.J.B. Bronswijk, and J. Halbertsma. 1988.
651 Modelling soil water dynamics in the unsaturated zone-State of the art. *Journal of*
652 *Hydrology*, 100, 69–111.
653 Feddes, R.A., P.J. Kowalik, and H. Zaradny. 1978. Simulation of field water use and crop
654 yield, John Wiley and Sons, New York, NY.

Freer, J., McDonnell, J.J., Beven, K.J., Brammer, D., Burns, D., Hooper, R. P., and Kendall, C. 1997. Topographic controls on subsurface storm flow at the hillslope scale for two hydrologically distinct small catchments. *Hydrological Processes*, 11, 1347–1352.

Freeze, R.A. 1972. Role of subsurface flow in generating surface runoff 1. Base flow contributions to channel flow. *Water Resources Research*, 8, 609–624.

Gardenas, A.I., J. Šimůnek, N. Jarvis, and M.Th. Van Genuchten. 2006. Two-dimensional modelling of preferential water flow and pesticide transport from a tile-drain field. *Journal of Hydrology*, 329, 647–660.

Gao, M., Li, H.-Y., Liu, D., Tang, J., Chen, X., Chen, X., Blöschl, G., and L.R. Leung. 2018. Identifying the dominant controls on macropore flow velocity in soils: A meta-analysis. *Journal of Hydrology*, 567, 590–604.

Gerke, H.H., and M.T. van Genuchten. 1993a. A dual-porosity model for simulating the preferential movement of water and solutes in structured porous media. *Water Resources Research*, 29, 305–319.

Gerke, H.H., and M.T. van Genuchten. 1993b. Evaluation of a first order water transfer term for variably saturated dual-porosity flow models. *Water Resources Research*, 29, 1225–1238.

Graham, C., and H.S. Lin. 2011. Controls and frequency of preferential flow occurrence at the Shale Hills Critical Zone Observatory: A 175 event analysis of soil moisture response to precipitation. *Vadose Zone Journal*, 10, 816–831.

Grayson, R., Blöschl, G., 2000. Spatial modelling of catchment dynamics. In: Grayson, R., Blöschl, G. (Eds.), Spatial Patterns in Catchment Hydrology: Observations and Modelling. Cambridge University Press.

Gu, W.Z., J.F. Liu, H.S. Lin, J. Lin, H.W. Liu, A.-M. Liao, N. Wang, W.Z. Wang, T. Ma, N. Yang, X.G. Li, P. Zhuo, and Z. Cai. 2018. Why hydrological maze: The hydropedological trigger? Review of experiments at Chuzhou Hydrology Laboratory. *Vadose Zone Journal*, 17, 170174. doi:10.2136/vzj2017.09.0174.

Guo, L., H.S. Lin, and J. Chen. 2014. Subsurface lateral flow network on a hillslope revealed by time-lapse ground penetrating radar. *Water Resources Research*, 50, 9127–9147.

Guo, L., H. Lin, B. Fan, J. Nyquist, L. Toran, G. Mount. 2019. Preferential flow through shallow fractured bedrock and a 3D fill-and-spill model of hillslope subsurface hydrology. *Journal of Hydrology*, 576, 430–442.

Haga, H., Y. Matsumoto, J. Matsutani, M. Fujita, K. Nishida, and Y. Sakamoto. 2005. Flow paths, rainfall properties, and antecedent soil moisture controlling lags to peak discharge

689 in a granitic unchanneled catchment. *Water Resources Research*, 41, W12410,
690 doi:10.1029/2005WR004236.
691 Hendrickx, J.M.H., and M. Flury. 2001. Uniform and preferential flow, mechanisms in the
692 vadose zone, Conceptual Models of Flow and Transport in the Fractured Vadose Zone,
693 National Research Council, National Academy Press, Washington, DC, pp. 149–187.
694 Hopp, L., and J.J. McDonnell. 2009. Connectivity at the hillslope scale: Identifying
695 interactions between storm size bedrock permeability, slope angle and soil depth.
696 *Journal of Hydrology*, 376, 378–391.
697 Kohne, J.M., B. Mohanty, J. Šimůnek, and H.H. Gerke. 2004. Numerical evaluation of a
698 second-order water transfer term for variably saturated dual-permeability models. *Water*
699 *Resources Research*, 40:W07409, doi:10.1029/2004WR003285.
700 Korres, W., T.G. Reichenau, P. Fiener, C.N. Koyama, H.R. Bogena, T. Cornelissen, R. Baatz,
701 M. Herbst, B. Diekkrüger, H. Vereecken, and K. Schneider. 2015. Spatio-temporal soil
702 moisture patterns-A meta-analysis using plot to catchment scale. *Journal of Hydrology*,
703 520, 326–341.
704 Larsson, M.H., and N.J. Jarvis, 1999. Evaluation of a dual-porosity model to predict field-
705 scale solute transport in a macroporous soil. *Journal of Hydrology*, 215, 153–171.
706 Lin, H. 2006. Temporal Stability of Soil Moisture Spatial Pattern and Preferential flow
707 Pathways in the Shale Hills Catchment. *Vadose Zone Journal*, 5, 317–340.
708 Lin, H. and X. Zhou. 2008. Evidence of preferential flow using soil hydrologic monitoring in
709 the Shale Hills catchment. *European Journal of Soil Science*, 59, 34–49.
710 Liu, H. and H.S. Lin. 2015. Frequency and control of preferential flow: from pedon to
711 catchment scales. *Soil Science Society of America Journal*, 79, 362–377.
712 Loague, K., C.S. Heppner, B.B. Mirus, B.A. Ebel, Q. Ran, A.E. Carr, S.H. BeVille, and J.E.
713 VanderKwaak. 2006. Physics-based hydrologic-response simulation: Foundation for
714 hydroecology and hydrogeomorphology. *Hydrological Processes*, 20(5), 1231–1237.
715 Loos, C., S. Gayler, and S. Priesack. 2007. Assessment of water balance simulations for large
716 scale weighing lysimeters. *Journal of Hydrology*, 335, 259–270.
717 Maxwell, R.M. 2020. Water colour and climate. *Nature Climate Change*, 102–103.
718 Maxwell, R.M., and S.J., Kollet. 2008. Interdependence of groundwater dynamics and land-
719 energy feedbacks under climate change. *Nature Geoscience*, 1, 665–669.
720 Melsen, L.A., Teuling, A.J., Torfs, P.J.J.F., Uijlenhoet, R., Mizukami, N., and Clark, M.P.
721 2016. HESS Opinions: The need for process-based evaluation of large-domain hyper-
722 resolution models. *Hydrology and Earth System Sciences*, 20, 1069–1079.

McCord, J.T., D.B. Stephens, and J.L. Wilson. 1991. Hysteresis and state-dependent anisotropy in modeling unsaturated hill slope hydrologic processes. *Water Resources Research*, 27, 1501–1518.

McDonnell, J.J., Sivapalan, M., Vaché, K., Dunn, S.M., Grant, G., Haggerty, R., Hinz, C., Hooper, R., Kirchner, J., Roderick, M.L., Selker, J., Weiler, M. 2007. Moving beyond heterogeneity and process complexity: a new vision for watershed hydrology. *Water Resources Research*, 43, W07301, DOI:10.1029/2006WR005467.

Mirus, B.B., B.A. Ebel, K. Loague, and B.C. Wemple. 2007. Simulated effect of a forest road on near-surface hydrologic response: Redux. *Earth Surface Processes and Landforms*, 32(1), 126–142.

Mirus, B.B., K. Loague, J.E. VanderKwaak, S.K. Kampf, S.J. Burges. 2009. A hypothetical reality of Tarrawarra-like hydrologic response. *Hydrological Processes*, 23(7), 1093–1103.

Newman, B.D., A.R. Campbell, and B.P. Wilcox. 1998. Lateral subsurface flow pathways in a semiarid ponderosa pine hillslope. *Water Resources Research*, 34, 3485–3496.

Nimmo, J.R. 2012. Preferential flow occurs in unsaturated conditions. *Hydrological Processes*, 26, 786–789.

Onda, Y., Y. Komatsu, M. Tsujimura, and J. Fujihara. 2001. The role of subsurface runoff through bedrock on storm flow generation. *Hydrological Processes*, 15, 1693–1706.

Rakovec, O., R. Kumar, S. Attinger, and L. Samaniego. 2016. Improving the realism of hydrologic model functioning through multivariate parameter estimation. *Water Resources Research*, 52, 7779–7792.

Saito, H., J. Šimůnek, and B.P. Mohanty. 2006. Numerical analysis of coupled water, vapor, and heat transport in the vadose zone. *Vadose Zone Journal*, 5, 784–800.

Schulz, K., R. Seppelt, E. Zehe, H.J. Vogel, and S. Attinger. 2006. Importance of spatial structures in advancing hydrological sciences, *Water Resources Research*, 42, W03S03, doi:10.1029/2005WR004301.

Scanlon, B.R., M. Christman, R. Reedy, I. Porro, J. Šimůnek, and G. Flerchinger. 2002. Intercode comparisons for simulating water balance of surficial sediments in semiarid regions. *Water Resources Research*, doi:10.1029/2001WR001233.

Salve, R., D.M. Rempe, and W.E. Dietrich. 2012. Rain, rock moisture dynamics, and the rapid response of perched groundwater in weathered, fractured argillite underlying a steep hillslope. *Water Resources Research*, 48, 1–25.

Sidle, R., S. Noguchi, Y. Tsuboyama, and K. Laursen. 2001. A conceptual model of preferential flow systems in forested hillslopes: evidence of self-organization. *Hydrological Processes*, 15, 1675–1692.

Šimůnek, J., N.J. Jarvis, M.T. van Genuchten, and A. Gardenas. 2003. Review and comparison of models for describing nonequilibrium and preferential flow and transport in the vadose zone. *Journal of Hydrology*, 272, 14–35.

Šimůnek, J., M.T. van Genuchten, and M. Sejna. 2006. The HYDRUS Software Package for Simulating Two- and Three-dimensional Movement of Water, Heat, and Multiple Solutes in Variably-Saturated Media: Technical Manual. Version 1.0. PC-Progress, Prague, Czech Republic.

Šimůnek, J., M.Th. van Genuchten, M. Sejna. 2016. Recent developments and applications of the HYDRUS computer software packages. *Vadose Zone Journal*. 15, http://dx.doi.org/10.2136/vzj2016.04.0033.

Sivakumar, B. 2004. Dominant processes concept in hydrology: moving forward. *Hydrological Processes*,18, 2349–2353.

Todd, M.S., P.R. Jeff, and M.H. George. 2000. Shallow subsurface storm flow in a forested headwater catchment: Observations and modeling using a modified Topmodel. *Water Resources Research*, 36(9), 2575–2586.

Tromp-van Meerveld, I., and M. Weiler. 2008. Hillslope dynamics modeled with increasing complexity. *Journal of Hydrology*, 361, 24–40. DOI: 10.1029/2007WR006299.

Tromp-van Meerveld, H.J. and J.J. McDonnell. 2006. Threshold relations in subsurface stormflow 1. A 147 storm analysis of the Panola hillslope. *Water Resources Research*, 42, W02410, doi:10.1029/2004WR003778.

Tromp-van Meerveld, H.J., N.E. Peters, J.J. McDonnell. 2007. Effect of bedrock permeability on subsurface stormflow and the water balance of a trenched hillslope at the Panola Mountain Research Watershed, Georgia, USA. *Hydrological Processes*, 21, 750–769.

Twarakavi, N.K.C., Šimůnek, J., Seo, H.S. 2008. Evaluating interactions between groundwater and vadose zone using HYDRUS-based flow package for MODFLOW. *Vadose Zone Journal*, 7, 757–768.

van Genuchten, M.T. 1980. A closed-form equation for predicting the hydraulic conductivity of unsaturated soils. *Soil Science Society of America Journal*, 44, 892–898.

van Genuchten, M.T., F.J. Leij, and S.R. Yates. 1991. The RETC code for quantifying the hydraulic functions of unsaturated Soils. Ver. 1.0 EPA Rep. 600/2-91/065. U.S. Salinity Lab., USDA-ARS, Riverside, CA.

Vereecken, H., J.A. Huisman, H.J. Hendricks Franssen, N. Brggemann, H.R. Bogena, S. Kollet, M. Javaux, J. van der Kruk, and J. Vanderborght. 2015. Soil hydrology: Recent methodological advances, challenges, and perspectives. *Water Resources Research*, 51, 2616–2633.

Vogel, H.-J., and K. Roth. 2003. Moving through scales of flow and transport in soil. *Journal of Hydrology*, 272, 95–106.

Weiler, M., and J.J. McDonnell. 2004. Virtual experiments: a new approach for improving process conceptualization in hillslope hydrology. *Journal of Hydrology*, 285, 3–18.

Whipkey, R.Z. 1965. Subsurface stormflow from forested slopes. *Bulletin-International Association of Scientific Hydrology*, 10, 74–85.

Zepp, H., J.L. Tang, and B. Zhang. 2005. A methodological framework for a multiscale study on hydrological processes and soil erosion in subtropical SE China. *Pedosphere*. 15, 695–706.

Zhao, Y., S. Peth, R. Horn, J. Krümmelbein, B. Ketzer, Y.Z. Gao, J. Doerner, C. Bernhofer, and X.H. Peng. 2010. Modelling grazing effects on coupled water and heat fluxes in Inner Mongolia grassland. *Soil and Tillage Research*, 109, 75–86.

Zhao, Y., J. Tang, C. Graham, Q. Zhu, K. Takagi, and H. Lin. 2012. Hydropedology in the ridge and valley: soil moisture patterns and preferential flow dynamics in two contrasting landscapes. In: Lin, Henry (Ed.), Hydropedology: Synergistic Integration of Soil Science and Hydrology. Academic Press.

All Figures and Tables.

Table 1 Soil and landscape features displayed for the monitoring sites 74, 54, 51, and 15 in the Shale Hills catchment of Pennsylvania.

Soil series	Site number	Landform position	Slope/%	Soil horizon	Sensor depth/cm	Depth to bedrock/cm	Rock fragment/%	Soil texture
Weikert	74	Nearly planar upslope	23.8	Oe-A	5	22		
				A	8		0	Silt loam
				A-CR	10		60	Silt loam
				CR	17		90	Silt loam
				R	37			
Rushtown	53	Swale, upslope	38.4	A	10	>150	5	Silt loam
				Bw1	22		5	Silt loam
				Bw2	44		5	Silt loam
				Bw3	73		5	Silty clay loam
				C	123		80	
Rushtown	51	Swale, midslope	13.1	Oe-A	5	>300		
				A	8		5	Silt loam
				A-Bw1	12		5	Silt loam
				Bw1	15		5	Silt loam
				Bw2	22		5	Silt loam
				Bw3	40		5	Silty clay loam
				BC	68		50	Silty clay loam
				BC-C1	92		50	Silty clay loam
				C1	122		80	
				C2	162		80	
Ernest	15	Valley floor	6.6	A	13	> 300	0	Silt loam
				AE-Bw	20		0	Silt loam
				Bt	41		0	Silty clay
				Bt-C2	52		0	Silty clay
				C2	72		80(soft)	Sandy loam
				C2-C3	85		0	Clay
				C4	109		90 (soft)	Sandy loam

Table 2 Hydraulic parameters for the different monitoring sites: (a) single-porosity model with van Genuchten-Mualem parameters obtained from inverse modeling with field data, (b) dual-porosity model parameters obtained from inverse modeling with field data (immobile water parameters indicated by subscript im, and mobile water parameters indicated by subscript mo). a_w is a first-order mass transfer coefficient.

Site	Soil depth (cm)	(a) single-porosity model						(b) dual-porosity model				
		θ_r (cm^3cm^{-3})	θ_s (cm^3cm^{-3})	α (cm^{-1})	n (-)	$K_s(K_v/K_h)$ (cm d^{-1})	l (-)	θr_{mo} (cm^3cm^{-3})	θs_{mo} (cm^3cm^{-3})	θr_{im} (cm^3cm^{-3})	θs_{im} (cm^3cm^{-3})	a_w ($cm^{-1}d^{-1}$)
74	0-5	0.020	0.260	0.247	1.523	316/80	0.5	0	0.160	0.020	0.100	1.839E-04
	5-15	0.000	0.290	0.036	1.714	3003/265	0.5	0	0.190	0.000	0.100	1.098E-03
	15-30	0.030	0.250	0.020	1.547	301/320	0.5	0	0.100	0.030	0.150	7.198E-01
	30-76	0.040	0.400	0.022	1.473	109/560	0.5	0	0.150	0.040	0.250	1.934E-04
53	0-10	0.000	0.440	0.007	2.277	1123/159	0.5	0	0.350	0.000	0.090	5.953E-04
	10-40	0.040	0.380	0.008	2.089	5/245	0.5	0	0.300	0.040	0.080	2.066E-05
	40-80	0.040	0.330	0.021	1.594	293/370	0.5	0	0.180	0.040	0.150	5.579E-03
	80-149	0.010	0.260	0.006	1.846	318/690	0.5	0	0.150	0.010	0.110	5.930E-04
51	0-10	0.030	0.400	0.080	1.580	150/116	0.5	0	0.360	0.030	0.040	2.000E-04
	10-30	0.050	0.450	0.011	3.461	602/270	0.5	0	0.350	0.000	0.150	9.301E-03
	30-50	0.030	0.330	0.012	2.278	144/2100	0.5	0	0.200	0.000	0.160	2.623E-03
	50-100	0.050	0.300	0.037	1.801	299/410	0.5	0	0.150	0.080	0.120	2.056E-03
	100-236	0.030	0.300	0.009	2.095	2/450	0.5	0	0.160	0.050	0.140	6.651E-03
15	0-20 20-52	0.050	0.450	0.023	2.228	27/170	0.5	0	0.390	0.050	0.060	5.390E-04
	52-83	0.080	0.430	0.013	1.962	2485/230	0.5	0	0.330	0.080	0.100	1.134E-05
	83-91	0.120	0.420	0.012	1.716	273/320	0.5	0	0.290	0.100	0.150	2.024E-04
	91-260	0.100	0.370	0.100	1.450	100/310	0.5	0	0.250	0.100	0.120	2.000E-04
	0-10	0.130	0.350	0.014	1.355	57/130	0.5	0	0.200	0.100	0.180	2.038E-04

Table 3 Design of the multi-dimensional, i.e., 1D, 2D, and 3D modeling approaches and its corresponding uncertainty comparisons used in the study. single-porosity model (VG), dual-porosity model (DP), fractured bedrock (FB), impermeable bedrock (IB), isotropy K_s (Iso) and anisotropy K_s (Ani). Y: available; N: not available.

Scale	soil hydraulic parameterization		K_s		boundary	
	VG	DG	Iso	Ani	IB	FB
2D (baseline)	Y	Y	Y	Y	Y	Y
1D	Y	N	Y	N	Y	N
3D	Y	N	Y	N	Y	N

Table 4 Nash–Sutcliffe efficiency (*NSE*) values and root mean square errors (*RMSE*) of the 1D, 2D, and 3D modeling approaches during the hydrological year 2007 at the sites 74 and 15 as used in the single-porosity model (VG), impermeable bedrock (IB), and Isotropy K_s. The model uncertainty comparisons included the corresponding 2D simulations of the dual-porosity model (DP), fractured bedrock (FB), and anisotropy K_s (Ani).

Site	soil	simulation using the single-porosity model (VG), impermeable bedrock (IB) and Isotropy K_s						model uncertainty comparisons					
	depth	*NSE*			*RMSE*			*NSE*			*RMSE*		
	(cm)	1D	2D	3D	1D	2D	3D	DP	FB	Ani	DP	FB	Ani
74	5	-0.319	0.122	**0.705**	0.045	0.021	0.021	-0.153	-0.282	0.220	0.020	0.050	0.023
	10	0.169	0.399	**0.737**	0.035	0.024	0.020	0.296	0.329	0.360	0.018	0.031	0.018
	17	-2.047	**0.534**	**0.646**	0.068	0.020	0.023	**0.623**	0.456	-2.223	0.017	0.029	0.18
	37	-2.538	-0.195	-0.087	0.036	0.021	0.020	0.475	-1.330	-16.823	0.017	0.029	0.019
51	18	-1.562	-1.026	0.312	0.067	0.059	0.034	0.239	0.498	-0.256	0.036	0.030	0.049
	40	-0.627	-0.307	0.439	0.042	0.050	0.025	0.191	**0.516**	-0.127	0.029	0.023	0.040
	92	-0.441	0.017	0.222	0.032	0.026	0.023	0.128	**0.567**	0.036	0.024	0.015	0.021
	162	-3.790	-2.558	-3.448	0.044	0.074	0.043	-2.015	-0.676	-2.874	0.035	0.026	0.040

(a)

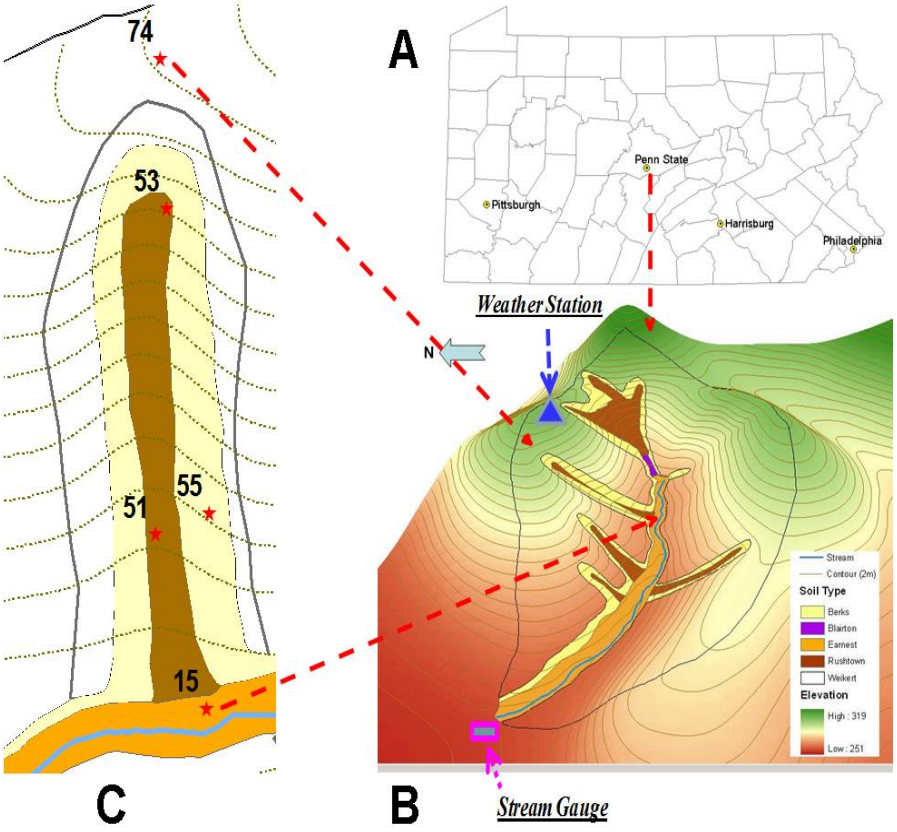

(b)

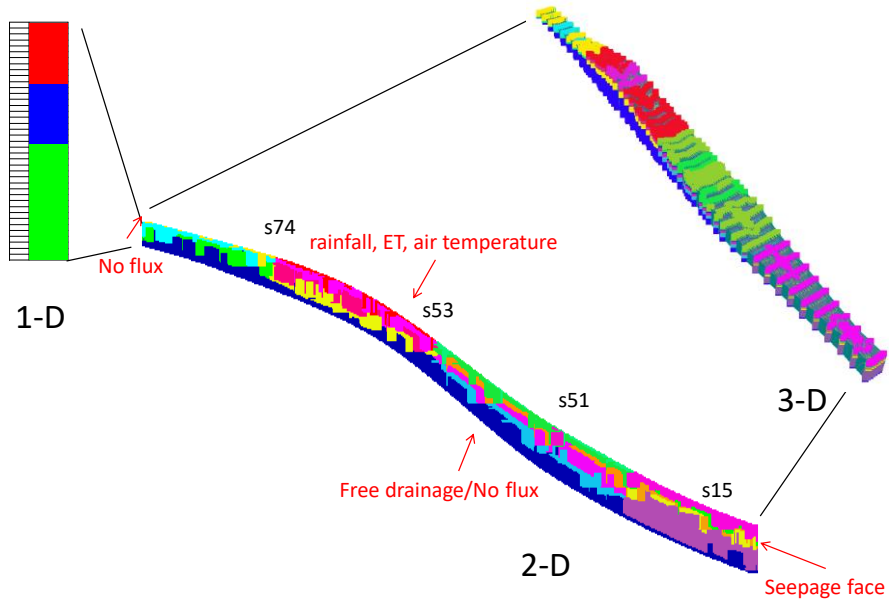

Figure 1. (a) Location (A) and shape (B) of the Shale Hills catchment, and the study hillslope (C), and (b) graphical representation of the HYDROUS-1D, -2D, and -3D simulation approaches used for the soil domain with 18 different soil materials as characterized by the different colors for the monitoring sites 74 (s74), 53 (s53), 51 (s51), and 15 (s15) with the applied boundary conditions.

(a)

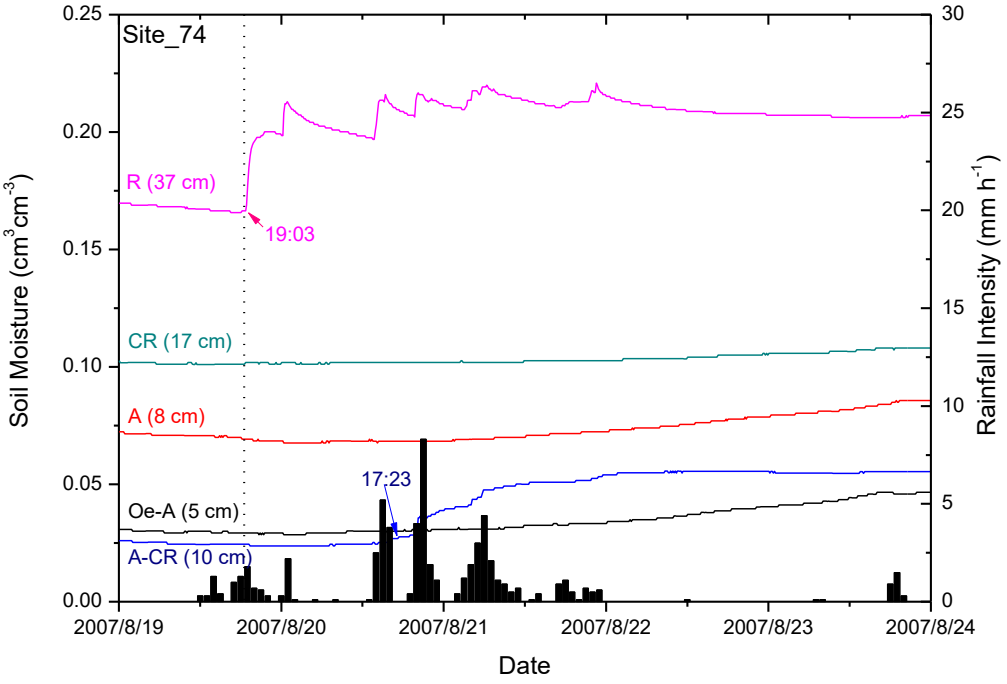

(b)

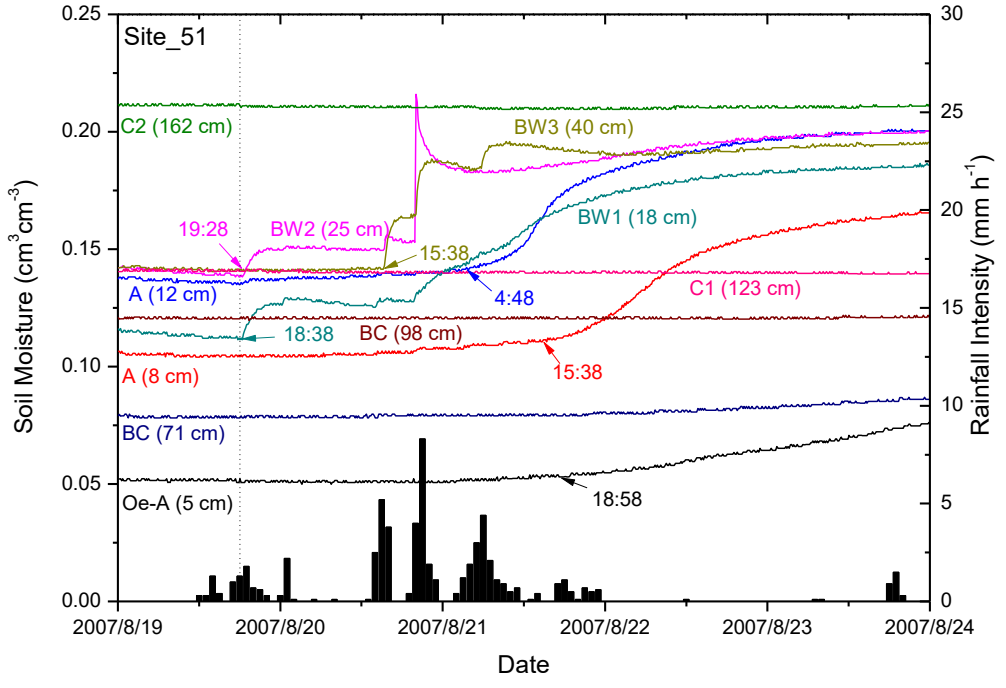

Figure 2. Minute-based volumetric soil moisture contents and rainfall intensities displayed over time during the drier period of August 19-24, 2007 at site_74 (a) and site_51 (b). The time at which soil moisture contents started to increase following a rainfall event is indicated by bold arrows. The different colored lines identify the soil horizons with the horizon layer in capital letters and the depth of soil moisture content in parenthesis.

(a)

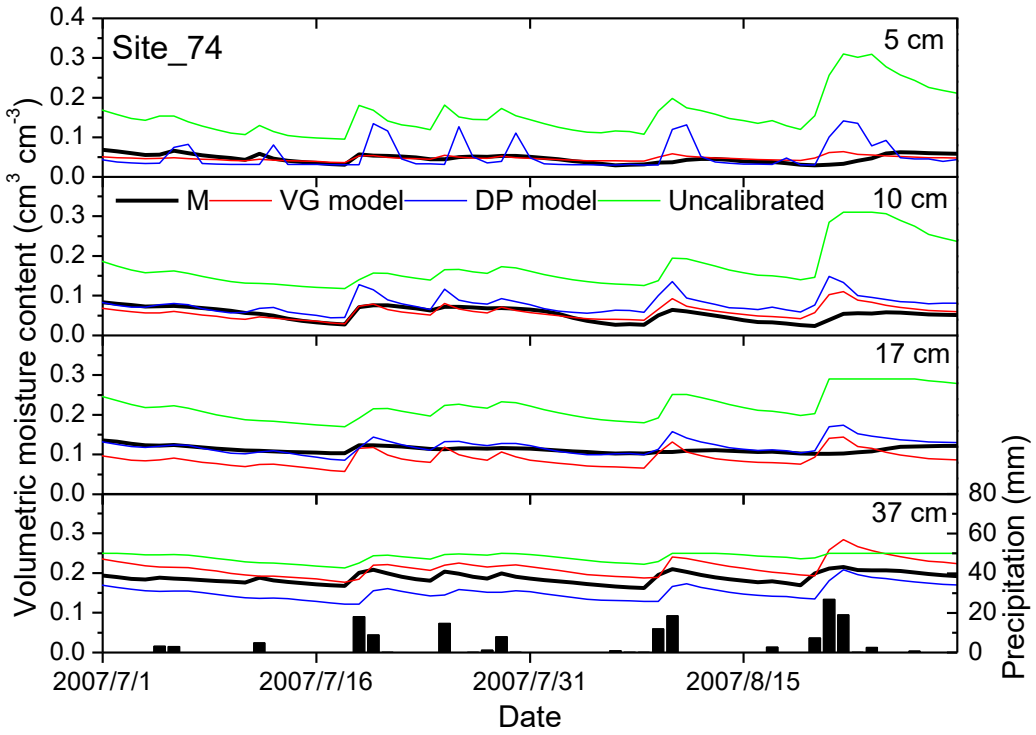

(b)

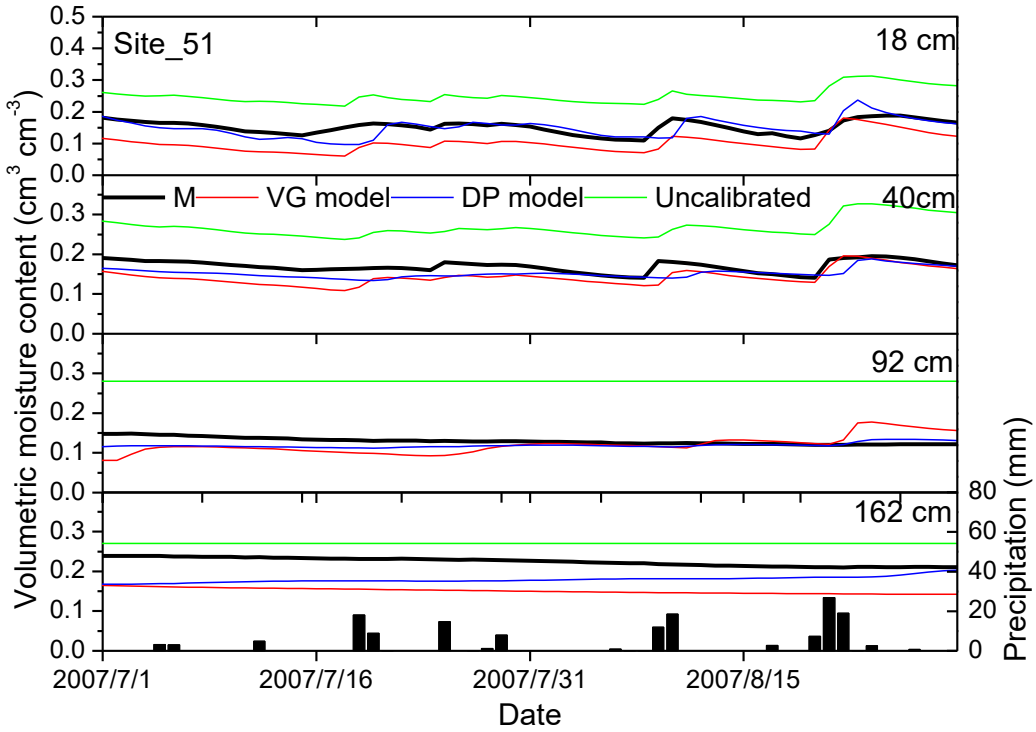

Figure 3. Comparison of the predicted and measured soil moisture values and rainfall quantities displayed over time for use in the HYDRUS-2D model calibrations at site 74 (a) and site 51 (b). uncalibrated: initial laboratory-measured hydraulic parameters.

(a)

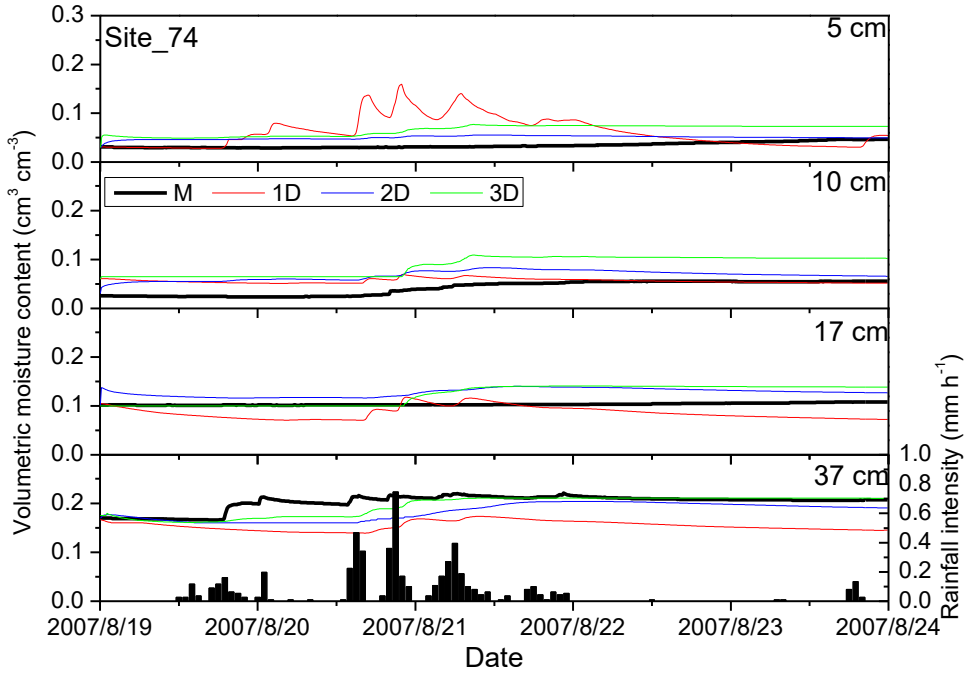

(b)

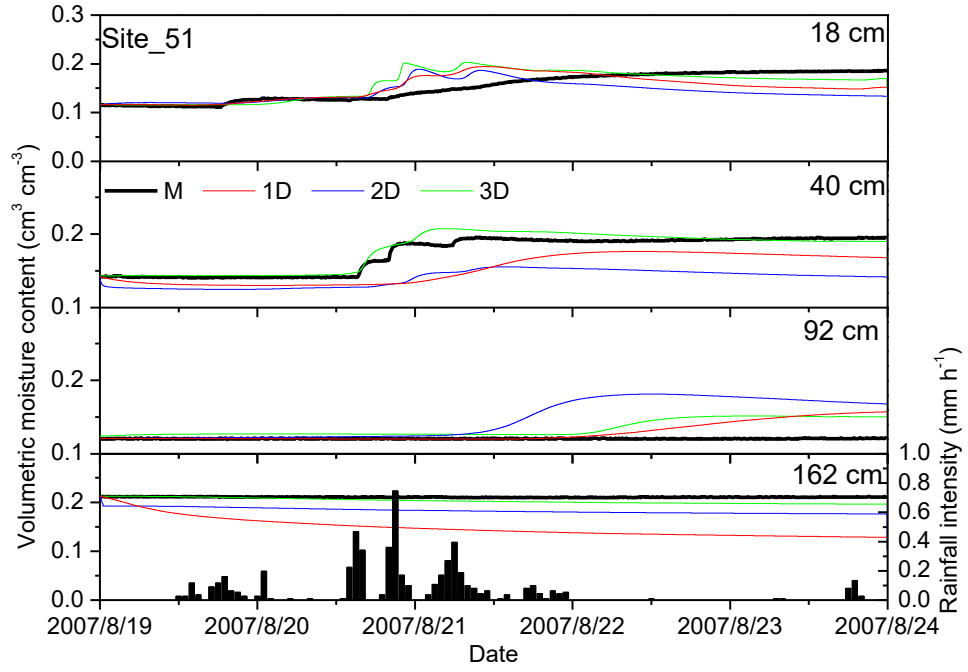

Figure 4. Measured (M) and predicted soil moisture values and rainfall intensities displayed over time during the drier period of August 19-24, 2007 at site_74 (a) and site_51 (b) by the HYDRUS-1D, -2D and -3D models.

(a)

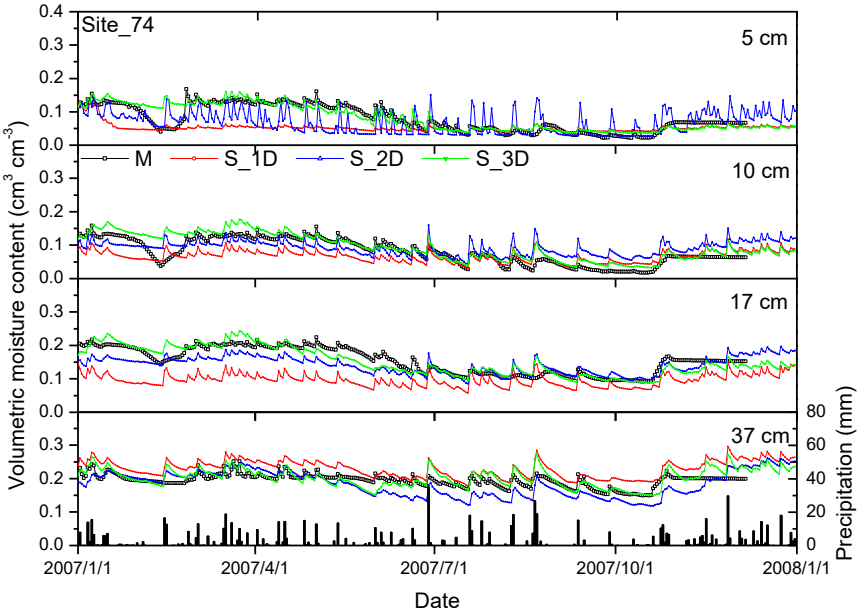

(b)

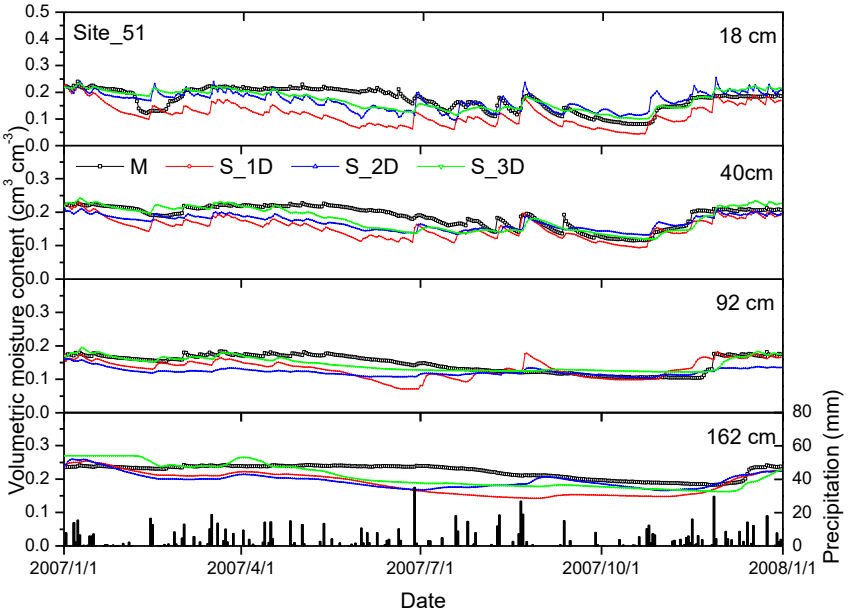

Figure 5. Measured (M) and predicted soil moisture values and rainfall intensities displayed over time in 2007 at site_74 (a) and Site_51 (b) by the HYDRUS-1D (S_1D), -2D (S_2D) and -3D (S_3D) models.

(a)

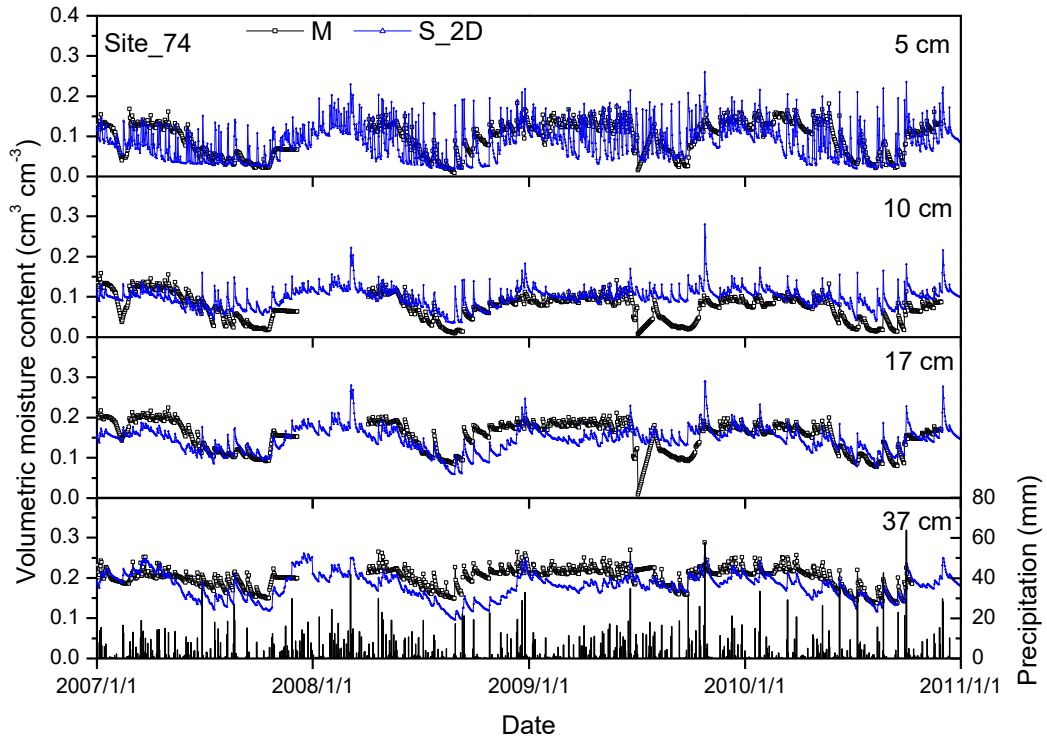

(b)

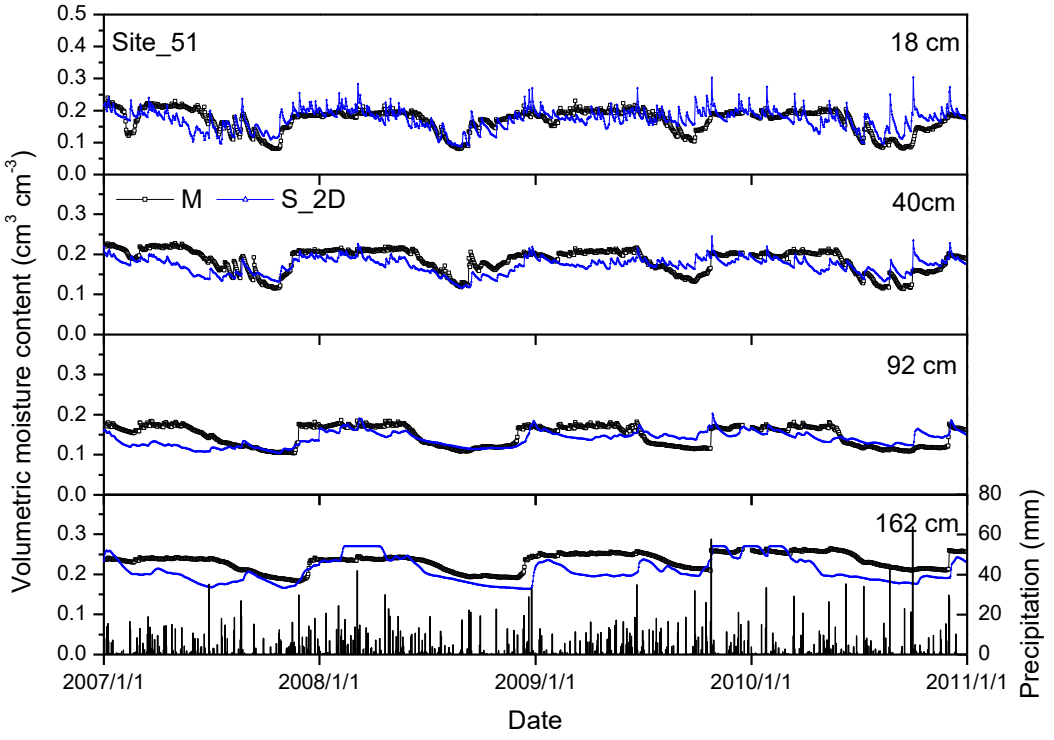

Figure 6. Measured (M) and predicted soil moisture values and rainfall intensities displayed over time in 2007-2010 for site_74 (a) and site_51 (b) by the HYDRUS- 2D model (S_2D).

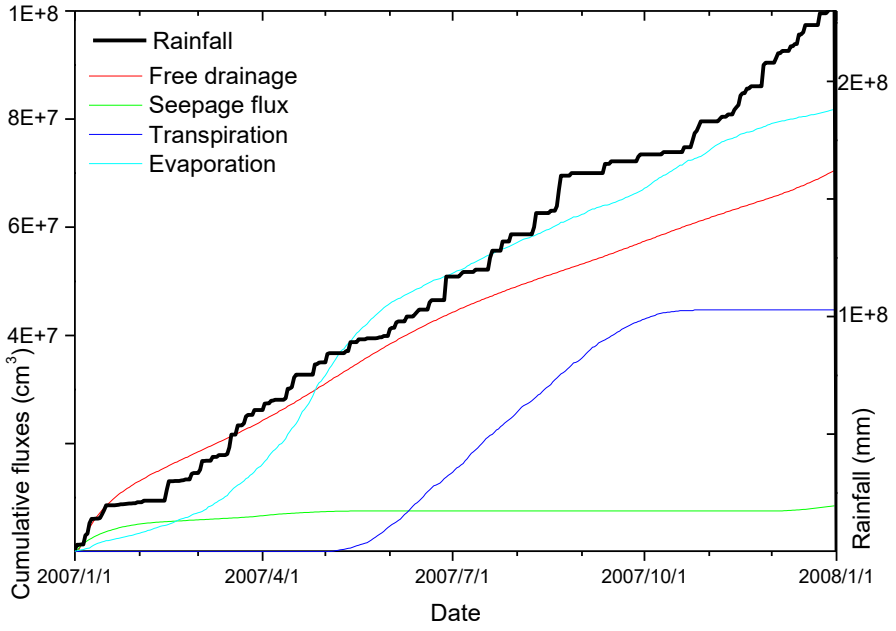

Figure 7. Cumulative fluxes of different terms of simulated water balances displayed over time for the studied area in 2007.

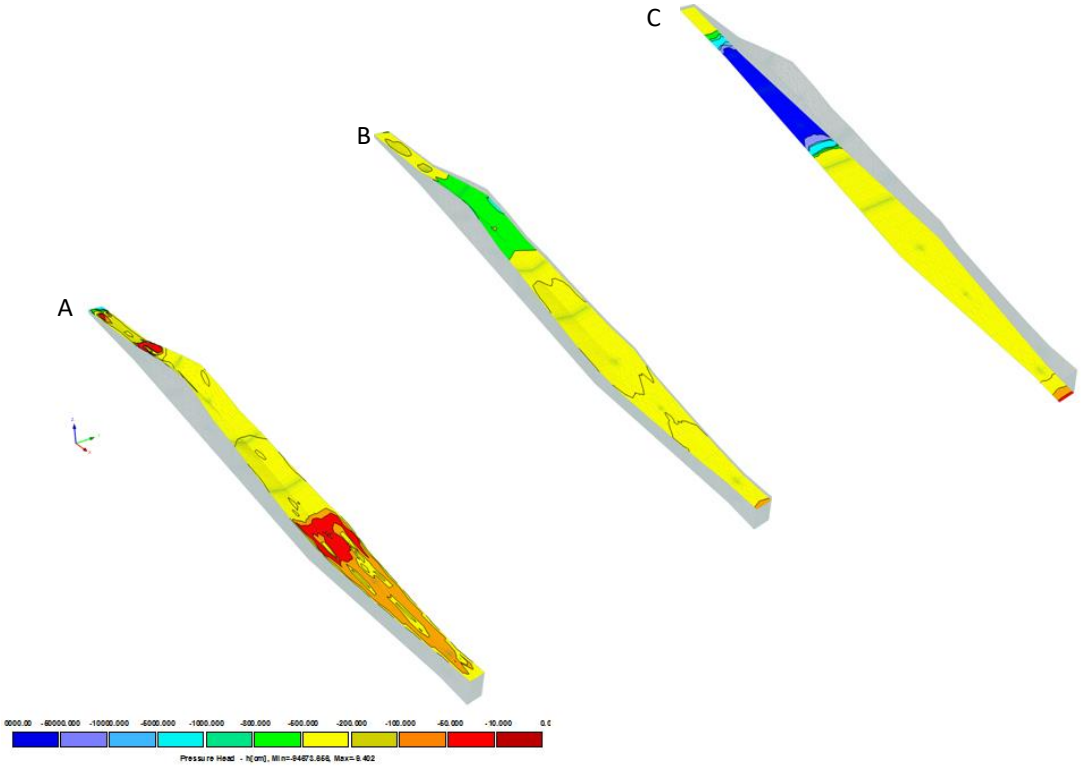

Figure 8. Snapshots of spatially variable pressure head at the 0-cm topsoil (A), the 40-cm subsoil (B), and the soil/bedrock interface (C) that were simulated by HYDRUS-3D for August 20, 2007.

(a)

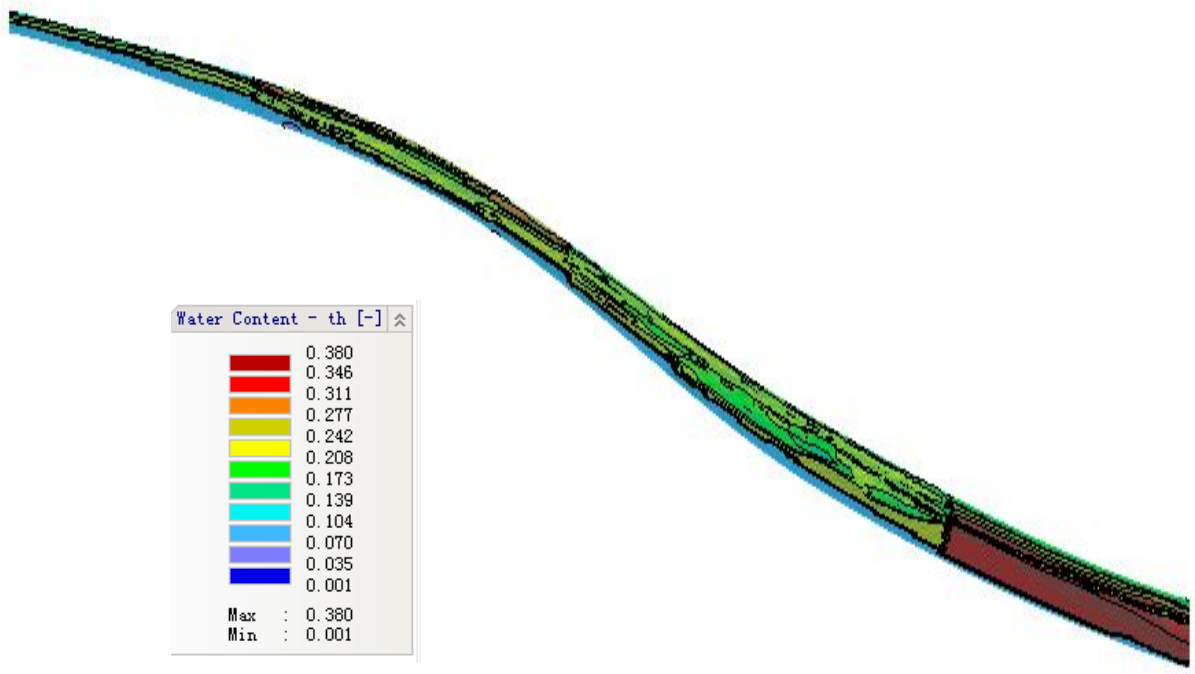

(b)

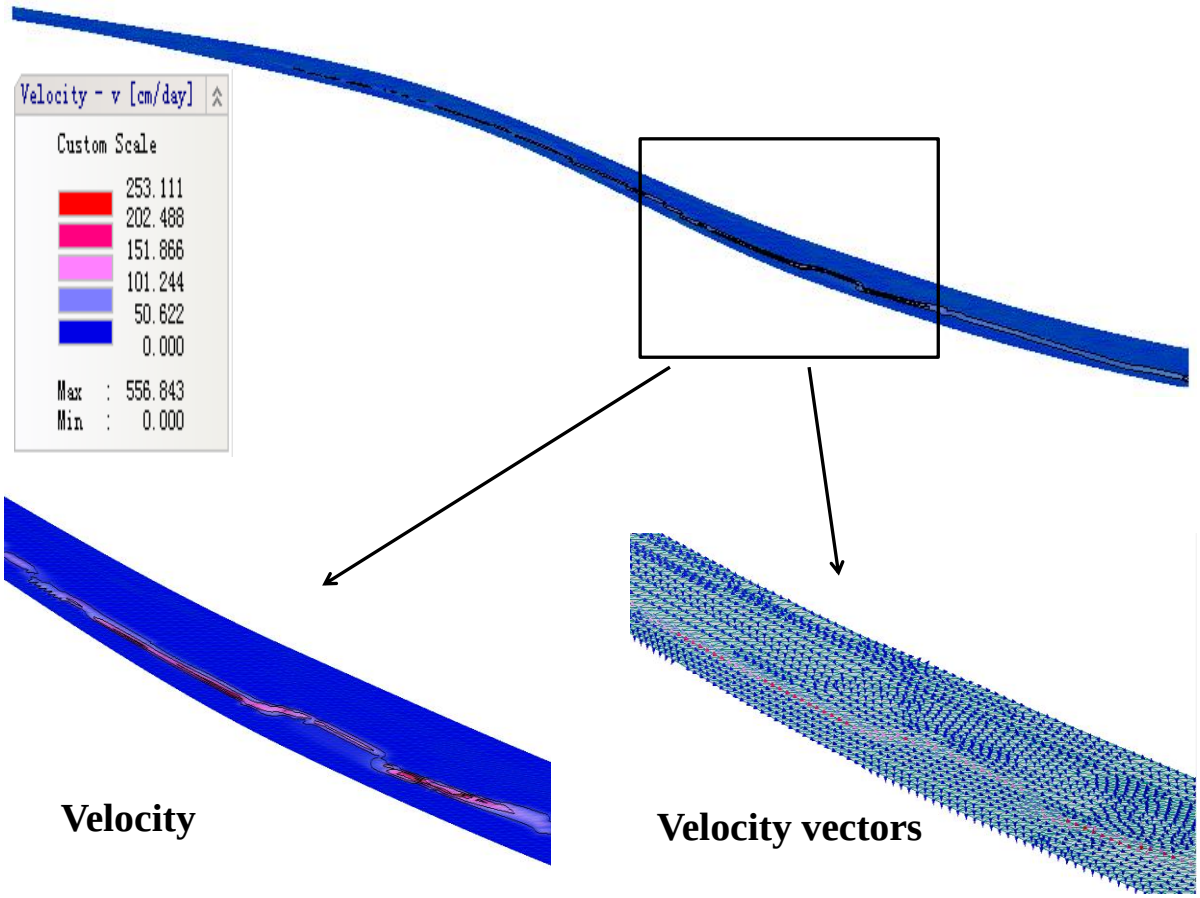

Figure 9. The 2D-distribution of (a) soil moisture content values and (b) water flux velocities displayed for August 20, 2007.

(a)

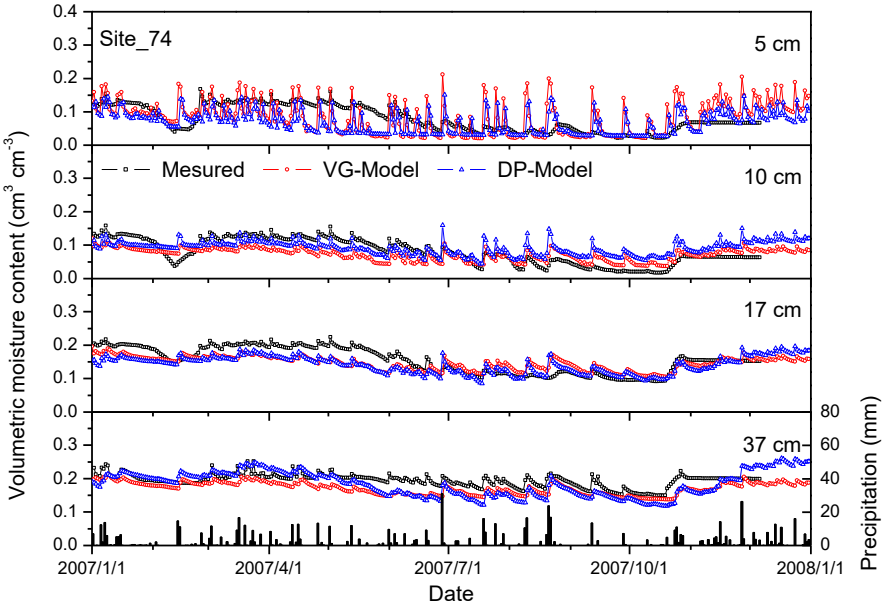

(b)

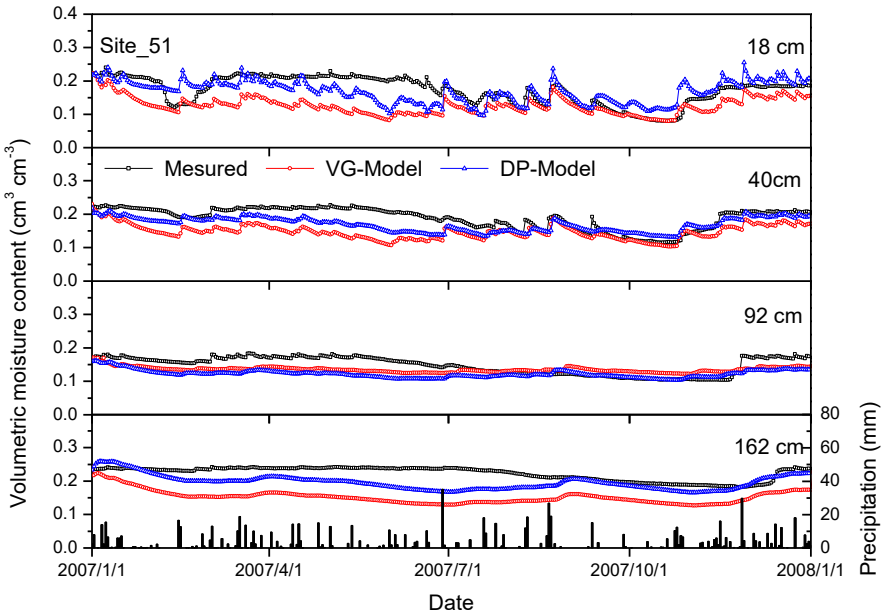

Figure 10. Comparisons between measured and predicted soil moisture values over time in 2007 for the single-porosity model (VG) and the dual-porosity model (DP) at site 74 (a) and site 51 (b) by the HYDRUS-2D model.

(a)

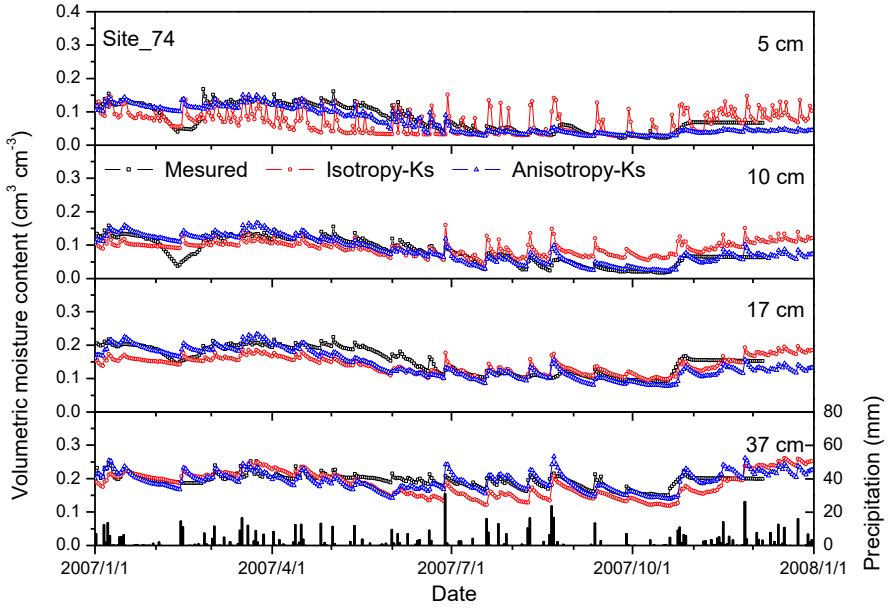

(b)

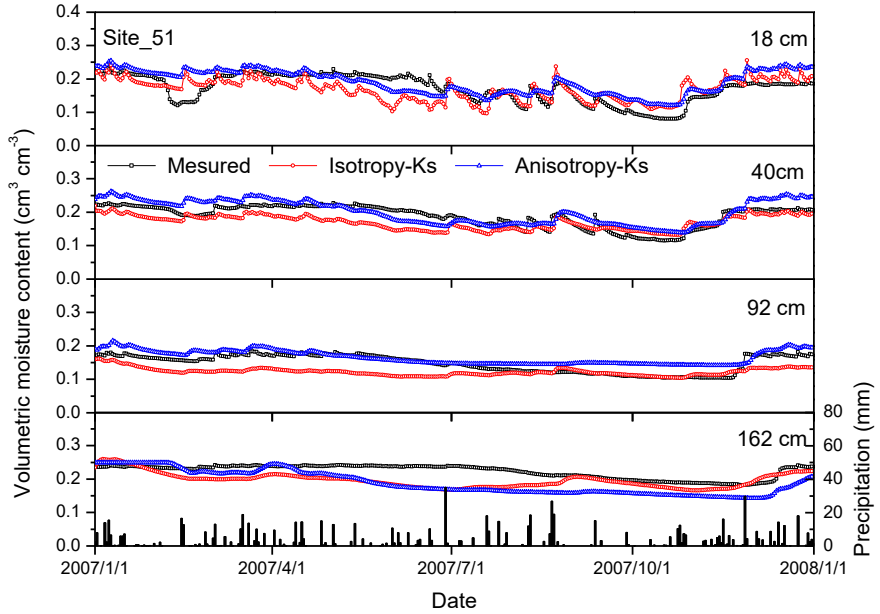

Figure 11. Comparisons between measured and predicted soil moisture values displayed over time in 2007 for isotropy-Ks and anisotropy-Ks at site 74 (a) and site 51 (b) by the HYDRUS-2D model.

(a)

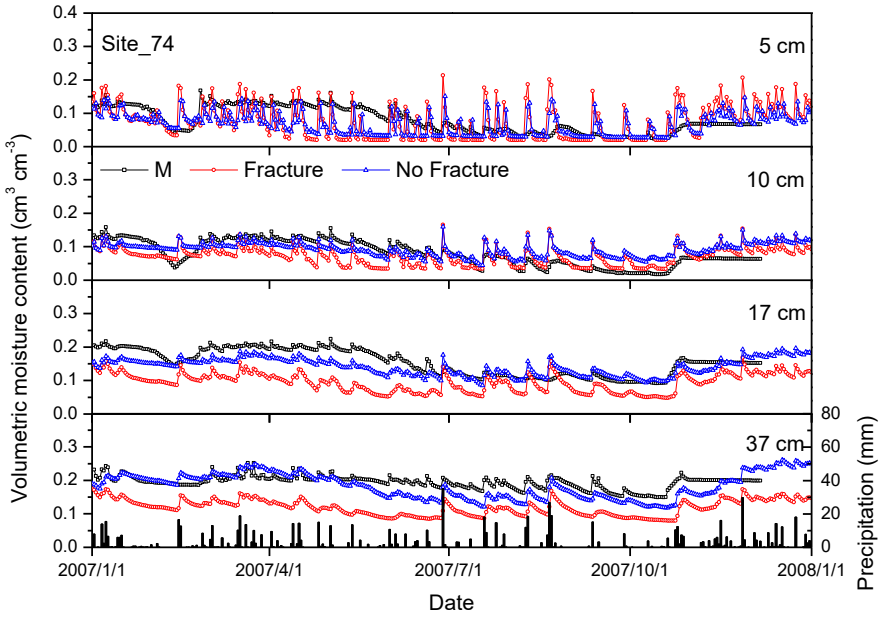

(b)

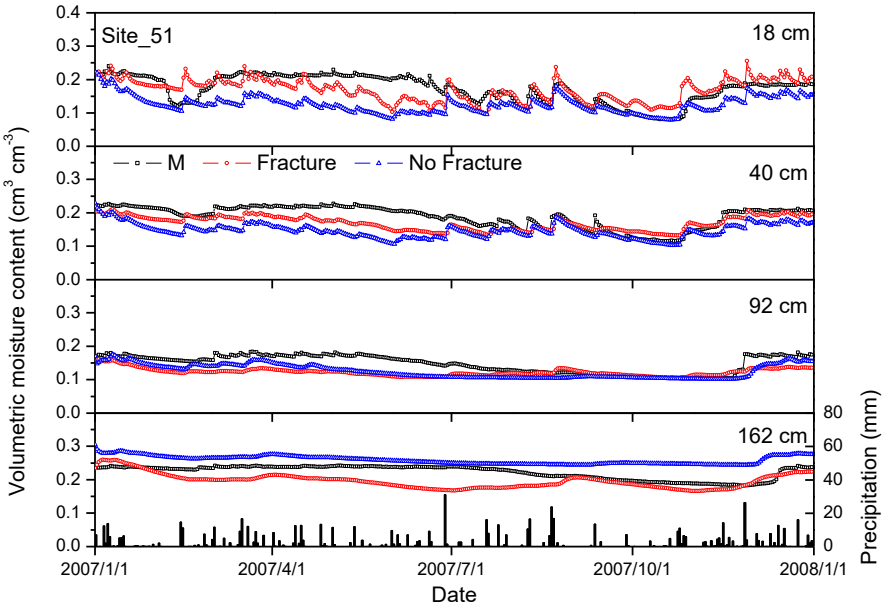

Figure 12. Comparisons between measured and predicted soil moisture values displayed over time in 2007 for permeable free drainage boundary condition (Fracture) and impermeable no-flux boundary condition (no fracture) for site 74 (a) and site 51 (b) by the HYDRUS-2D model.

(a)

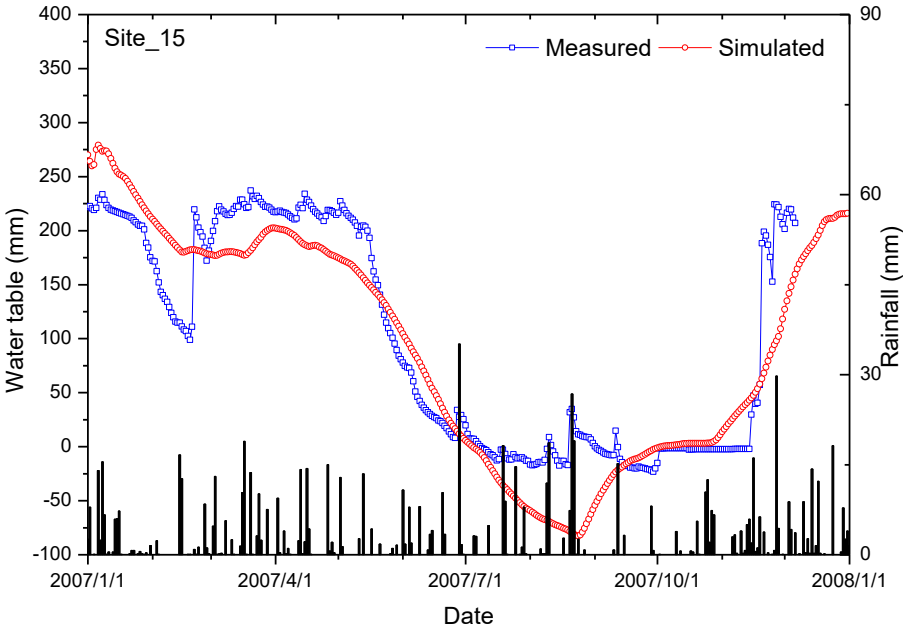

(b)

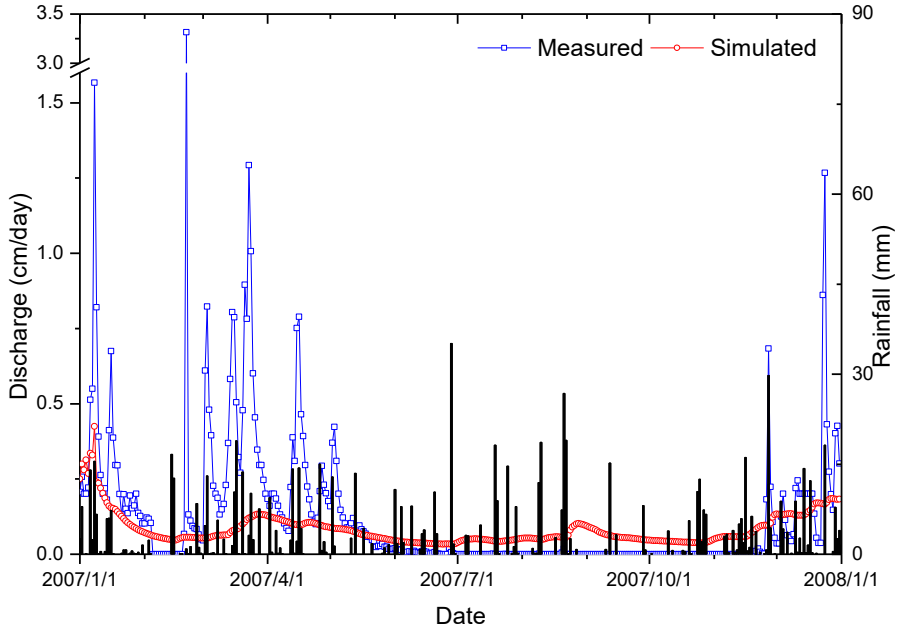

Figure 13. Comparisons between measured and simulated water tables for site 15 (a) and the measured discharge at the outlet of the catchment and simulated discharge for the sub-catchment evaluated during this study (b) with rainfall quantity distribution as a reference.

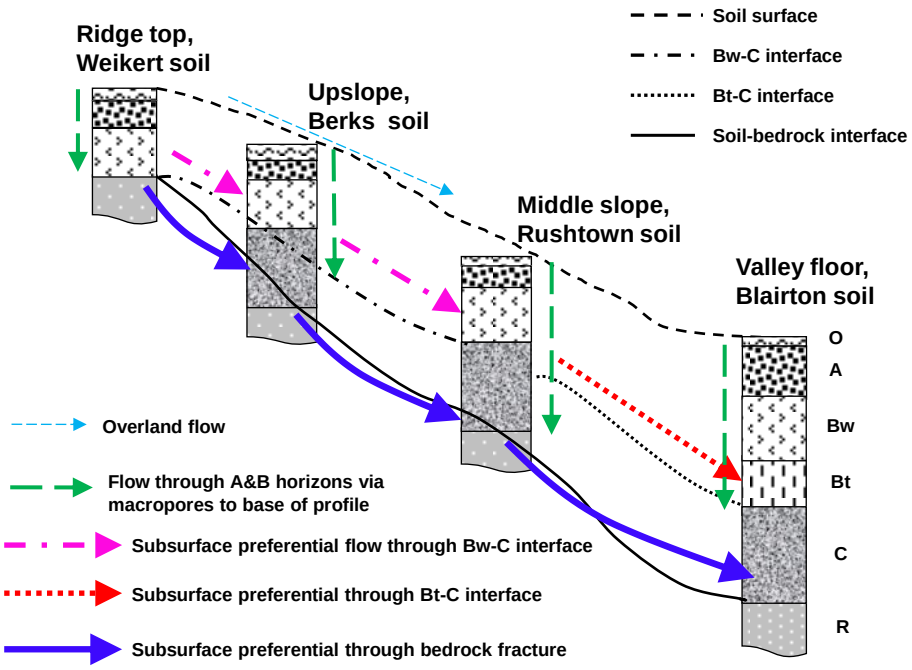

Figure 14. Conceptual diagram showing several potential subsurface preferential flow pathways along a hillslope in the Shale Hills catchment. The soil series and soil horizons are indicated for each landscape position, which is referenced in Table 1.